Construction and Building Materials 312 (2021) 125292

Contents lists available at ScienceDirect

Construction and Building Materials

journal homepage: www.elsevier.com/locate/conbuildmat

# The hybrid effects of basalt and PVA fiber on properties of a cementitious composite: Physical properties and non-destructive tests

Şükrü Özkan [a,*], Ömer Çoban [b]

[a] Isparta University of Applied Sciences, Technical Sciences Vocational School, Department of Construction, Isparta 32260, Türkiye
[b] Bilecik Şeyh Edebali University, Vocational School, Department of Construction, Bilecik 11230, Türkiye

ARTICLE INFO

*Keywords:*
Basalt fiber
Cementitious composite
Density
Hybrid
Non-destructive test
PVA fiber
Water absorption capacity

ABSTRACT

This study aimed to experimentally examine the physical properties and non-destructive properties of cementitious composites for different hybrid basalt and PVA fiber contents. The total fiber content of 2% was formed with five different proportions of PVA fiber and basalt fiber. Within the scope of the experimental studies, various mechanical (compressive strength and elasticity modulus), durability (capillary water absorption and water absorption), physical (apparent void volume and bulk density), non-destructive (ultrasonic pulse velocity and Schmidt rebound hammer) and microstructural (scanning electron microscopy) tests were carried out to investigate the properties of the produced hybrid fiber reinforced composites. The results showed that the water absorption capacity and water absorption coefficient by capillarity values decreased while the hardened composite density values increased as the basalt fiber ratio increased in the mixtures. The maximum ultrasonic pulse velocity values were obtained from P0B100 (consisting of only 100% basalt fiber) samples with the highest Schmidt rebound hammer values of 4.11 km/s and 32, respectively.

## 1. Introduction

The number of the studies conducted on environmentally friendly and sustainable building materials has increased dramatically in recent years. The use of fibers obtained from natural and renewable sources in cementitious composites has gained importance in terms of obtaining superior mechanical properties and providing higher shrinkage and expansion resistance. In fiber reinforced cementitious composites (FRCC), short fiber types such as PVA, Polypropylene, carbon, glass, steel, basalt are used to improve the various properties of the composite [1–6]. However, some fibers require more energy during the production phase. As a result, more carbon emission occurs. In addition, it is a drawback that the raw materials required for the production of fibers to be used in cementitious composites production are not available everywhere or are limited. The increasing awareness of sustainability in the construction industry contributes to the discovery, development and inclusion of materials with more environmentally friendly production processes.

Basalt fibers are environmentally sustainable materials as they are obtained as a result of processing basalt rock derived from local and natural resources; they reduce $CO_2$ emission during the production phase and are produced with less energy due to their natural state. Because of these properties, basalt fibers are a green alternative to petrochemical-based and synthetic-based fibers [7–11].

The positive results obtained by singly use of basalt fiber and PVA fiber in cementitious composites [12–15] and other materials (geopolymer composite [16], polymer composite [17], fiber reinforced cement-stabilized macadam [18] etc.) were effective in used to improve some physical, durability and mechanical properties of cementitious composites by benefiting the positive synergistic effect of these two fiber species.

Moreover, in usage of the basalt fiber in the ECC mixtures as hybrid with together PVA fiber, it has been effective to reduce the cost increase resulting from PVA fiber that hinders widespread use of the ECCs in construction applications and to develop the physical and durability properties of the ECCs by benefitting from the superior mechanical and physical properties of the basalt fibers.

It is a common problem that the penetration of harmful substances causes deterioration. The transport and diffusion phenomena that constitute this problem cause the service life of concrete to be shortened by the penetration of harmful substances into the concrete. The water absorption ability/capacity of the hardened concrete affects the

* Corresponding author at: Isparta University of Applied Sciences, Vocational School of Technical Sciences, Department of Construction, West Campus PB, 32260 Isparta, Turkey.
*E-mail addresses:* sukruozkan@isparta.edu.tr (Ş. Özkan), omer.coban@bilecik.edu.tr (Ö. Çoban).

https://doi.org/10.1016/j.conbuildmat.2021.125292
Received 20 April 2021; Received in revised form 3 October 2021; Accepted 16 October 2021
Available online 5 November 2021

resistance and strength of the concrete against abrasive physical and chemical events that concrete may expose to during its service life. Both the water absorption and permeability of cementitious composites depend on the total amount of voids in the hardened composite structure and the relationships between the voids. The addition of basalt fiber to cementitious composites contributes to the reduction of the void content [19], so that the physical and chemical damage of the material can be reduced. The pore structures in hardened mortar become more disconnected because of the pore-blocking effect of the fibers, which leads to less capillary porosity and lower water penetration into mortars [20]. Superior impermeability feature contributes to the development of durability by preventing the rust of mortars by harmful substances. Jiang et al., [20] stated that the addition of PP fiber and basalt fiber to the repair mortars contributed to the superior abrasion resistance, lower drying shrinkage, and the increase in freeze-thaw and impermeability resistance of the mixtures. Compared to the water penetration depth of 13.80 mm of the reference mixture, penetration depths of PP fiber and basalt fiber reinforced mortars with 2.6 kg/m$^3$ fiber content were found to be 4.1 mm and 5.6 mm, respectively.

It was determined in previous studies that water absorption values vary depending on the type of fiber used in cementitious composites and the amount of fiber per unit volume [21–23]. In addition, filling of the matrix pores due to the ongoing hydration process has been effective in reducing water absorption [24]. Pakravan et al. used PVA fiber and ground rice husk (GRH) in hybrid combinations with the aim of producing low cost and high quality cementitious composites. As a result of the experimental studies, it was determined that the water absorption values of hybrid fiber mixtures increased by 12–18% compared to mono fibers [21]. Wang et al. [25] studied changes in water absorption of 0%, 0.05%, 0.1%, 0.2% and 0.3% basalt fiber reinforced concrete for 90 days in 5.0% sodium sulfate solution and clean water. The experimental studies showed that the water absorption rates of basalt fiber reinforced concrete samples soaked in clean water were lower than those under the influence of sulfate. In both conditions, the water absorption values of the samples were observed to show a tendency to decrease first and then increased. Additionally, the samples with 0.1 % basalt fiber showed the highest performance under sulfate erosion condition in reducing water absorption by limiting the void structure. Şahmaran and Li [26] investigated the fly ash effect on the durability of ECCs using a series of transport properties tests, including the sorptivity test. As a result of the experimental studies, they found that depending on the increase in the number of micro cracks in ECCs, the amount of water absorption (sorptivity) increased. In the study conducted by Hanafi et al. [27] to investigate the physical, mechanical and durability properties of basalt fiber reinforced cement paste composites, the researchers used basalt fibers in three different volume fractions (0.3%, 0.75% and 1.5%) and in three different curing times (7, 28 and 56 days). As a result of the study, it was found that density, void volume and water absorption values tended to decrease at later curing ages. It was also observed that the porosity values tended to increase with the addition of 0.3% basalt fiber by volume, and the water absorption values showed a tendency to increase with the addition of 0.75% basalt fiber by volume.

Depending on the density of the fibers in hybrid fiber or single fiber mixtures, the density of the cementitious composite material also varies [21,28,29]. It should be noted that low density reduces the durability of concrete products. Therefore, it is of great importance to consider all the properties of concrete before conducting construction work. In some cases, constructors have to increase the cement mortar density. Whether the steel inside the reinforced concrete structure is corroded depends on the environment and the structure of the concrete itself. In order to prevent or at least delay the corrosion, concrete with a suitable density, low permeability and no voids as possible should be made.

Due to their low cost and simplicity, non-destructive testing techniques are used in structural investigations, as a supportive of destructive methods, to evaluate conventional concrete quality and mechanical properties [30–34]. Another function of these techniques is to help the determination of the relative quality and homogeneity of concrete by providing information about the presence of cracks and voids. Although there are many non-destructive methods used in applications, Schmidt rebound hammer (SRH) and ultrasonic pulse velocity (UPV) methods are the two methods widely used in laboratory and field applications. UPV is used to determine various parameters such as determination of concrete quality, correlations related to concrete strength, dynamic modulus of elasticity and determination of poisson's ratio [35]. In the UPV method, pressure waves are created in the concrete by applying ultrasonic pulse to one side of the concrete to be tested. The test device used in the UPV method determines the duration that is required for the ultrasonic waves to cover the distance between the transmitted surface and the receiving surface. In this way, the transition velocity of ultrasonic pulses through the concrete sample can be calculated, and from here, comments can be made on the concrete strength and some other properties. UPV values decrease due to factors such as the increase in the pores, internal cracks and the unit weight in the cementitious structure.

The components of cementitious composite such as type of aggregate, addition and water cement ratio can be noted as the factors affecting UPV [36–38]. Type of fibers used in cementitious composites is another factor affecting UPV [39–41].

The SRH test is another non-destructive test method used in structural investigations. Schmidt test hammer enables the measurement of the surface hardness of the hardened concrete and the estimating the strength of the concrete in this way [42–45]. This mass, which works with a spring-loaded system, rebounds, and how much the mass bounces through the indicator on the instrument can be measured numerically. Another use of the concrete hammer test is to understand to which extend the strength development of concrete samples subjected to freeze–thaw effect is affected by cycles [34]. Some factors such as cement type, cement ratio, aggregate type, surface variety of the sample, surface humidity, carbonation effect, concrete age, initial hardening rate, curing conditions and compression has great impact on the rebound values [46–48]. Studies on SRH test in non-destructive methods used in fiber-reinforced cementitious composites have shown in the literature that various aggregates can affect the surface hardness of cementitious mortars and concretes, although not as much as the UPV test [49–52]. Within the knowledge of the authors, it has been determined that there are very few studies examining the effect of single or hybrid fiber reinforced cementitious composites on SRH [53]. Therefore, the current study aims to investigate the hybrid effect of basalt and PVA fibers used as reinforcement on SRH, and therefore it was aimed to fill the gap in the literature.

SRH and UPV measurements in cementitious composites will differ from normal concrete due to some unique properties of this material. Some parameters that make cementitious composites different from concrete can be shown as the reasons why SRH and UPV measurements in cementitious composites, and therefore their correlations with compressive strength differ from normal concrete. These parameters are;

In terms of the type of aggregate used in mixtures: Unlike normal concrete, the absence of coarse aggregates in the content of cementitious composites has led to the absence of discontinuities in the microstructure compared to normal concrete [54].

In terms of density and water absorption capacity: In order to improve the toughness of cementitious composites, the micron-sized aggregate types used in the content according to the micromechanical design principles make the matrix structure more compact and dense. The decreasing water absorption capacity with increasing density that increases SRH and UPV values in cementitious composites will differ from normal concrete [55].

In terms of fibers used in cement-based composites: Unlike normal concrete, the use of various types and amounts of fibers in cementitious composites to prevent the brittleness of the densified matrix [15], provides positive changes in non-destructive test parameters such as UPV and SRH, and mechanical properties, due to their effect on the density of the matrix structure and the void structure.

In terms of water-binder ratio: The low water/cement ratio used in cementitious composites to provide a good balance between fresh and hardened properties and to contribute to strength development also helps to reduce capillary pores. In addition, the low water/cement ratio used in cement-based composites, unlike concrete, is a useful property for maintaining the consistency of the mixture and facilitating the distribution of fiber, which allows obtaining high SRH and UPV values [56,57].

When the literature is examined, it is seen that various studies are conducted on the use of UPV in concrete within the knowledge of the authors [54,58,59]. In cementitious composites, it is seen that UPV test is used in a limited way in order to follow the self-healing processes, the presence of pores and internal cracks in the composite structure [31–34]. Additionally, there are very few studies on cementitious composites produced with the hybrid use of PVA and basalt fiber, and it has been determined that these studies are generally related to the mechanical properties of the composite [60–62]. Therefore, the use of both UPV and SRH tests as non-destructive methods in cementitious composites where basalt and PVA fiber are used as hybrid and the examination of the physical properties of these hybrid composites constitute the originality of this study.

There are close relationships between the mechanical properties of building materials and their physical properties. Therefore, the mechanical properties of the materials can be developed by improving the physical properties. In this study, it is aimed to determine how the addition of basalt and PVA as hybrid fibers to cementitious composites affected the physical and durability properties such as bulk density, pore structure and water absorption properties. In addition, non-destructive methods such as SRH and UPV were used to evaluate the quality of composites produced.

## 2. Experimental studies

### 2.1. Materials

ASTM C150 [63] Type I Portland cement (CEM I 42.5 R) was utilized to produce hybrid ECC mixtures. Its specific gravity and surface area were 3.16 g/cm$^3$ and 3440 cm$^2$/gr, respectively. Table 1 contains information about the chemical composition of cement, as well as its physical and some mechanical properties.

Moreover, class F fly ash (FA) that meets the requirements specified in ASTM C618 (Standard Specification for Coal Fly Ash and Raw or Calcined Natural Pozzolan for Use in Concrete) [64] containing 1.16% CaO was utilized. Quartz sand (QS) with a maximum particle size of 150 μm, water absorption capacity of 0.3%, and specific gravity of 2.60 g/cm$^3$ was also used. The chemical compositions of fly ash and quartz sand are given in Table 2. In addition, Fig. 1 demonstrates the laser diffraction particle size distribution curves for OPC, FA, and QS.

PVA and basalt fiber utilized as microfiber in the novel hybrid mixtures were straight fibers with a diameter of 39 μm and a length of 8 mm for PVA fiber, and a diameter of 13–20 μm and a length of 12 mm for basalt fibers. The PVA fiber was surface-coated by hydrophobic oil (1.2% by weight) for the purpose of decreasing the fiber/matrix interfacial bond strength. Table 3 contains detailed information on the fiber characteristics. Additionally, Fig. 2 presents the photomicrograph of PVA and basalt fiber. Fibers were chosen by taking into account their reinforcing characteristics, as indicated in Table 3, which demonstrates that PVA and chopped basalt fibers have good tensile strength and Young's modulus, and the fibers in question were added as 2% by volume of the composite mix. A modified polycarboxylate-based polymer type superplasticizer additive (SP) was used to arrange the workability of cement-based mixtures. The superplasticizer additive used in experimental studies is a liquid chemical additive with a pH value of 3–7 and a specific gravity of about 1.10 ± 0.02 kg/l.

**Table 1**
Chemical compositions and physical characteristics of ordinary Portland cement as given by the manufacturer.

| Chemical composition of ordinary Portland cement | | ASTM C150 | Physical characteristics of ordinary Portland cement | | ASTM C150 |
|---|---|---|---|---|---|
| Constituents | (%) | | | | |
| CaO | 63.65 | | Volume expansion (mm) | 0.3 | <0,8 |
| $SiO_2$ | 19.87 | | Fineness (90 μ, %) | 0.10 | |
| $Al_2O_3$ | 4.11 | | Fineness (200 μ, %) | 1.10 | |
| $Fe_2O_3$ | 3.44 | | Specific surface area (cm$^2$/g) | 3340 | >160 |
| MgO | 1.61 | <6 | Initial setting times (min) | 144 | >45 |
| $SO_3$ | 2.68 | <3 | Final setting times (min) | 240 | <375 |
| $Cl^-$ | 0.004 | | | | |
| $K_2O$ | 0.48 | | Specific gravity (g/cm$^3$) | 3.12 | |
| $Na_2O$ | 0.12 | | | | |
| Loss of ignition | 2.20 | <3 | | | |
| Insoluble matter | 0.40 | <0.75 | | | |
| **Mechanical Characteristics of Ordinary Portland Cement (MPa)** | | | | | **ASTM C150** |
| 7-day flexural strength (MPa) | | 5.8 | 7-day compressive strength (MPa) | 39.3 | >19 |
| 28-day flexural strength (MPa) | | 7.2 | 28-day compressive strength (MPa) | 50.6 | |

**Table 2**
The chemical characteristics of fly ash and quartz sand

| Chemical composition (%) | Fly ash | ASTM C618 | Quartz sand |
|---|---|---|---|
| CaO | 1.16 | | 0.02 |
| $SiO_2$ | 61.72 | | 99.79 |
| $Al_2O_3$ | 20.13 | | 0.06 |
| $Fe_2O_3$ | 7.46 | | 0.02 |
| MgO | 1.80 | <5 | 0.01 |
| $SO_3$ | 0.22 | <5 | – |
| $K_2O$ | 1.88 | | 0.01 |
| $Na_2O$ (Alkalies) | 2.57 | | 0.02 |
| Free CaO | 0.071 | | |
| $Cl^-$ | 0.015 | | |
| Loss of ignition | 2.99 | <6 | 0.07 |
| $SiO_2 + Al_2O_3 + Fe_2O_3$ | 89.31 | >70 | – |
| 28-days index of activity | 81.9 | >75 | |
| Fineness, ≥45 μm (%) | 16.4 | ≤34 | |

### 2.2. Mixture proportions and mixing

Mixing all the mix ingredients, presented in Table 4, was performed in a planetary mixer with a capacity of 0.02 m$^3$. ECC mixtures were produced by keeping the water-to-binding materials (PC + FA) ratio (W/CM), fly ash to Portland cement ratio (FA/PC), and sand to binding materials ratio (S/CM) constant at 0.26, 1.2, and 0.36, respectively. A superplasticizer was utilized at varying doses, in accordance with the increase in fiber volume, for the purpose of increasing workability. The quantity of the superplasticizer primarily depended on the target slump of 40 ± 5 cm (without fibers) and 20 ± 5 cm (with fibers).

To control the workability of various ECC mixtures, a polycarboxylate-based superplasticizer (SP) was added by weight according to ASTM specifications C494 (Standard Specification for Chemical Admixtures for Concrete) [65]. The proportions of the hybrid ECC mixtures that were tested are presented in Table 4. The PVA fiber content is represented by the first number in the mixture label, and the

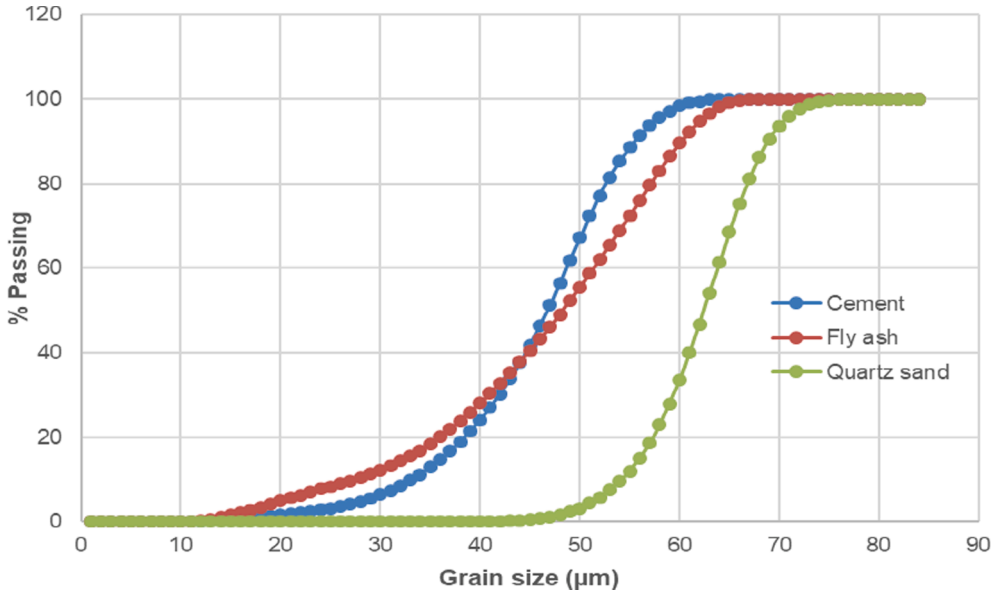


**Fig. 1.** Particle size distributions of cement, fly ash, and quartz sand.

**Table 3**
Specifications of PVA and basalt fiber as provided by the producer.

| Fiber type | Tensile strength (MPa) | Diameter (μm) | Length (mm) | Elastic modulus (GPa) | Elongation (%) | Specific gravity (gr/cm$^3$) |
|---|---|---|---|---|---|---|
| PVA | 1620 | 39 | 8 | 42.8 | 6.0 | 1.3 |
| Basalt | 2500 | 13–20 | 10–14 | 89 | 3.15 | 2.8 |

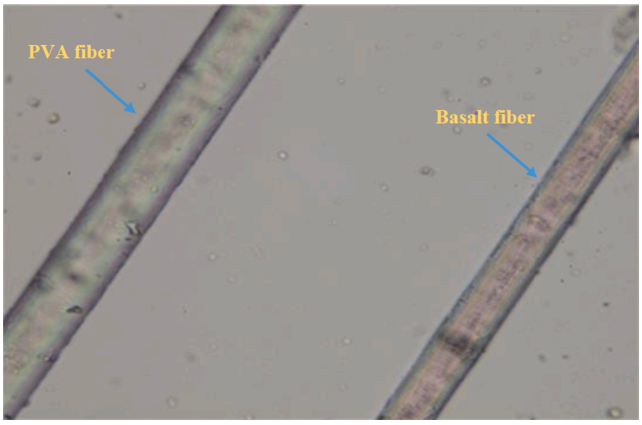


**Fig. 2.** Comparison of the images of PVA and basalt fibers under the microscope.

basalt fiber content is represented by the second number in the mixture label. For instance, P75B25 indicates that the total fiber amount (2% by volume or 26 kg/m$^3$ by weight) is composed of 75% PVA and 25% basalt fiber. To prevent inhomogeneity of the material, in the mix design, a 2% fiber content by volume in excess of the computed critical fiber content was usually utilized. The above-mentioned decisions were taken through the ECC micromechanics material design theory and were experimentally shown to yield good ECC characteristics [66].

Cement, fly ash, and silica sand were primarily mixed for about one and half minute at a low speed. Then water and water-reducing admixture was added to the dry mixture was performed, and the resulting mixture was mixed for subsequent 3 min. After obtaining consistent mixture, PVA and basalt fibers were added together slowly into the mortar mixture until the uniform distribution of all fibers in the cement paste was achieved. The entire mixing process usually lasted approximately 10 min. The composite was cast in plastic molds. Following the surface finishing, a polyethylene sheet was used to cover the samples for the purpose of preventing moisture loss, and they were kept under room temperature for a period of 24 h before demolding. After demolding was completed, the samples were cured in water at 23 °C ± 2 °C for up to 28 days.

**Table 4**
The mix design of the hybrid engineered cementitious composite (by weight).

| Mix code | W/BM[a] (Cement + Fly ash) | Sand/BM (Cement + Fly ash) | Fly ash/ Cement | Cement (kg/m$^3$) | Fly ash | Sand | Water | PVA fiber | Basalt fiber | SP[b] |
|---|---|---|---|---|---|---|---|---|---|---|
| P100B0 (Reference) | 0.26 | 0.36 | 1.20 | 571 | 685 | 455 | 331 | 26.00 | 0 | 4.9 |
| P75B25 | 0.26 | 0.36 | 1.20 | 571 | 685 | 455 | 331 | 19.50 | 6.50 | 4.95 |
| P50B50 | 0.26 | 0.36 | 1.20 | 571 | 685 | 455 | 331 | 12.90 | 13.10 | 4.95 |
| P25B75 | 0.26 | 0.36 | 1.20 | 571 | 685 | 455 | 331 | 6.30 | 19.70 | 4.95 |
| P0B100 | 0.26 | 0.36 | 1.20 | 571 | 685 | 455 | 331 | 0 | 26.00 | 4.95 |

[a] BM: Binding material,
[b] SP: Superplasticizer additive

### 2.3. Sample preparation

The preparation of the mixtures was performed following a typical ECC mixing procedure [8]. For each mixture, eight 100x75x50 mm prism samples were cast for unit weight, apparent porosity, water absorption, and capillary water absorption tests, three 100x75x50 mm prism samples were cast for ultrasonic pulse velocity tests, and three 360x75x50 mm prism samples were cast for the Schmidt rebound hammer test measurement. Demolding of all samples was performed following 24 h of casting, and then they were cured in water at 23 ± 2 °C until the age of 28 days, according to ASTM C 192 [67].

### 2.4. Experimental methods for determining mechanical, physical and non-destructive properties

#### 2.4.1. Compressive strength

The compressive strength test was conducted at the end of the 28th day using a 2000 kN capacity compressive tester on 50 mm cubic samples of different mixtures based on the provisions of ASTM C109 [68].

#### 2.4.2. Modulus of elasticity

The elasticity modules of the samples were determined according to Eq. (1) using the values found from the unit weight and UPV test.

$$E = (10^5 \times V^2) \times (\Delta/9.81) \quad (1)$$

where E represents modulus of elasticity (GPa), V represents ultrasonic pulse velocity (km/s) and Δ represents unit weight (g/cm$^3$).

#### 2.4.3. Bulk density, apparent void volume, water absorption

Density is a significant physical property for engineered cementitious composites. The physical characteristics of newly developed composites such as bulk density (BD), apparent void volume (AVV), water absorption (WA), and capillary water absorption (CWA), and the nondestructive characteristics of newly developed composites such as Schmidt rebound hammer tests (SRH) and ultrasonic pulse velocity (UPV) were tested at the age of 28 days after curing in water in the laboratory environment at 23 ± 3 °C and 25 ± 5% RH. The properties of these experiments were determined using Archimedes' principle by means of water-saturated weights at the end of 24 h, suspended weights in water, and weights after the sample was dried to a constant weight. The physical characteristics of composites were tested according to Standard ASTM C642-13 [69], and prismatic samples with the dimensions of 75 × 100 × 50 mm were utilized to test the physical characteristics (According to ASTM C642 –13, the volume of tested composite samples was>350 cm$^3$). Prismatic test samples with the same dimensions were also used for ultrasonic pulse velocity tests.

The composites' apparent void volume (AVV), bulk density (BD), and water absorption (WA) were acquired from the average of eight test samples for each condition, and physical properties were obtained using Eqs. (2)–(4) in accordance with the procedures indicated by ASTM C642-13 [69].

$$AVV(\%) = [(m_{sat} - m_{dry}) / (m_{sat} - m_i)] \times 100 \quad (2)$$

$$BD(g/cm^3) = [(m_{dry} / m_{sat} - m_i)] \times 1 \quad (3)$$

$$WA(\%) = [(m_{sat} - m_{dry})/m_{dry}] \times 100 \quad (4)$$

where $M_{sat}$ refers to the saturated sample's mass with a dry surface, $M_{dry}$ refers to the dry sample's mass following 48 h at the temperature of 105 °C, $M_i$ refers to the mass of the sample immersed in water, and ρ refers to the bulk density of water (1 g/cm$^3$) [69].

#### 2.4.4. Capillary water absorption test (Sorptivity)

A method for capillary water absorption properties was determined according to BS EN 772-11 [70]. After drying the samples to a constant mass, the samples to be used in the capillary water absorption test were placed on L-shaped strip elements in a container, as shown in Fig. 3. Then a surface of HECC samples was immersed in water for a particular period of time, and it was observed that the mass increased. The shortest period of immersion is typically one hour, as indicated by BS EN 772-11 [70]. A schematic representation of the experimental setup for the capillary water absorption test is shown in Fig. 3.

The coefficient of capillary water absorption of masonry materials is usually determined at 10, 30, 60, and 90 min [71]. Eq. (5) presented below was used to calculate the capillary water absorption coefficient of HECC samples according to BS EN 772-11 [70].

$$C_{w,s} = \left(m_{s_0,s} - m_{dry,s}\right) / \left(As \cdot \sqrt{tso}\right) \times 10^6 \quad (5)$$

where $C_w$ represents the water absorption coefficient (g/m$^2$ × s$^{0.5}$), $M_{S0,S}$ represents the mass of the sample in grams after soaking for time t, (g), $M_{dry,s}$ represents the mass of the sample after drying, (g), $A_s$ represents the gross area of the face of the sample immersed in water, (mm$^2$), and $t_{S0}$ represents the time of soaking, (s).

#### 2.4.5. Ultrasonic pulse velocity test

The measurement of the samples' ultrasonic pulse velocity (UPV) was performed at the age of 28 days. Prisms with the dimensions of 75x100x50 mm were used with a 100 mm path length. The prisms utilized for the measurement of the UPV were under the completely saturated surface dry condition (SSD). An Ultrasonic Non-Destructive Digital Tester with a precision of 0.1 μs was used to measure the samples' ultrasonic wave velocity values. A transducer with a 55 kHz vibration frequency was utilized. A through-transmission technique was employed to measure the sound transit times (t, μs) of HECC samples in accordance with ASTM C 597-09 [72]. The representative experimental setup for the ultrasonic pulse velocity test is shown in Fig. 4.

After taking the average of three readings for each sample, and the ultrasonic wave velocity (Vs, km/s) was computed by using the Eq. (6) presented below:

$$V = L/T \quad (6)$$

where V refers to the ultrasonic pulse velocity (km/s), L refers to the distance between centers of transducer faces (mm), and T refers to the taken time (μs).

#### 2.4.6. Schmidt rebound hammer test

The surface hardness of HECC samples was measured by a standard rebound hammer (N-type Schmidt hammer) in accordance with ASTM C 805 [73]. Ten readings were made on the samples with a Schmidt hammer. The surface hardness reading was performed at an angle of α = 90°when the composite surface was dry in accordance with the principles specified in the ASTM C 805 standard [73]. The Schmidt rebound hammer test of the samples was conducted at the age of 28 days. Prisms with the dimensions of 360x75x50 mm were used for the test. The *R* number was computed as the average of 10 measurements taken from the four opposite surfaces of each of the three prismatic samples, and

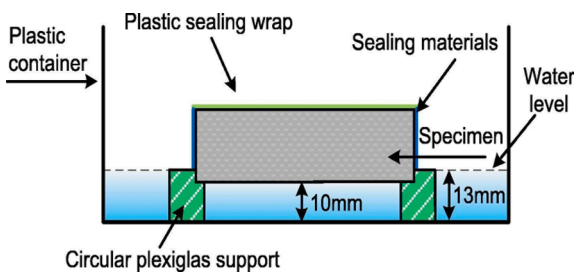


**Fig. 3.** Schematic representation of the capillary water absorption test setup.

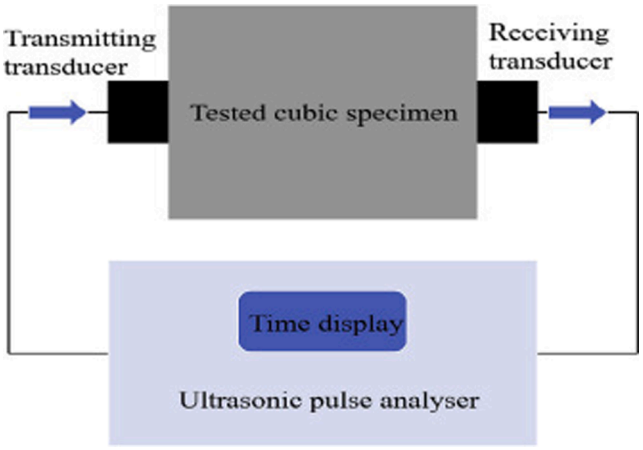


**Fig. 4.** Schematic representation of the UPV test setup.

pulse velocity (V) as the average of the two measurements, taken from the two opposite surfaces of each of the three prismatic samples.

Finally, in the following sections, experimental results obtained from different tests have been presented graphically to conduct meaningful interpretations.

## 3. Results and discussion

### 3.1. Compressive strength

The 28-day compressive strength values of hybrid basalt and PVA fiber reinforced cementitious composites are graphically presented in Fig. 5. In mixtures where the fiber content of 2% by weight consists of hybrid basalt and PVA fiber, 28-day compressive strength values of mixtures increase due to the increase in basalt fiber content. The highest values of compressive strength were obtained from the P0B100 mixture, in which the fiber content of 2% by weight consists of 100% basalt fiber. The lowest values of compressive strength were obtained from the reference mixture in which the 2% fiber content consists of only PVA fiber. According to the reference mixture, P75B25, P50B50, P25B75 and P0B100 mixtures showed an increase in compressive strength of 4%, 9%, 12% and 16%, respectively.

It is a known fact that fiber distribution has an effect on strength development and mechanical properties [74–78]. Since the cementitious mixture is water-based, the homogeneous distribution of the fibers increases as the hydrophilicity of the fibers increases [79,80]. The fact that the improvement of the strength values with the increase of basalt fiber can be resulted by the contribution of the hydrophilic structure of the basalt fiber [81–84] to a better fiber distribution due to the effect of facilitating fiber distribution [84]. In applications, the fiber distribution is affected by factors such as fiber properties (diameter, length and volumetric ratio in mix), flow properties of the matrix, method of placement and shape of the mold [85]. Another effect of basalt fiber on strength development is the fiber elastic modulus. The high modulus of elasticity (89 GPa) of basalt fiber contributes to the stiffer structure of the cementitious composite to which basalt fiber is added, thus the composite exhibits higher compressive strength [62].

In addition, Basalt fibers can be easily dispersed in the matrix without losing their shape and without causing segregation due to their flexible and hydrophilic structure [84]. Basalt fibers dispersed in the pores can improve the properties of the interface transition zone. Such a distribution allows basalt fibers, which contribute to the strength development with the effect of its high modulus of elasticity, to form a three-dimensional spatial load-bearing skeleton in the cementitious matrix [60,86,87]. By forming load-bearing skeletons of basalt fibers, it is ensured that the tension distribution improves, the crack driving force decreases, and the formation and development of microcracks is limited [86]. It has been stated in previous studies that when the volume fraction of basalt fibers in hybrid blends exceeds a certain ratio, it has a positive effect on the formation of the fiber spatial skeleton [12,62].

### 3.2. Modulus of elasticity

The modulus of elasticity values of the test samples were determined according to Eq. 1 given in Section 2.4.2, depending on the UPV and unit weights. The determined values are presented in Fig. 6. As seen in the figure, since the elastic modulus is a function of the compressive strength, the elastic modulus test results are compatible with the compressive strength test results [88].

While the E-modulus of the reference mixture was found as 28.69 GPa, it was also recorded as the lowest modulus of elasticity. Among the hybrid samples, the highest modulus of elasticity was obtained as 36.88 GPa from the samples coded P0B100 where 2% total fiber content consisted of only basalt fiber. As seen in Fig. 6, the modulus of elasticity values tend to increase with the increase in the amount of basalt fiber and with the decrease in the amount of PVA fiber in hybrid fiber blends. The reason for this increase is that high UPV values are measured due to

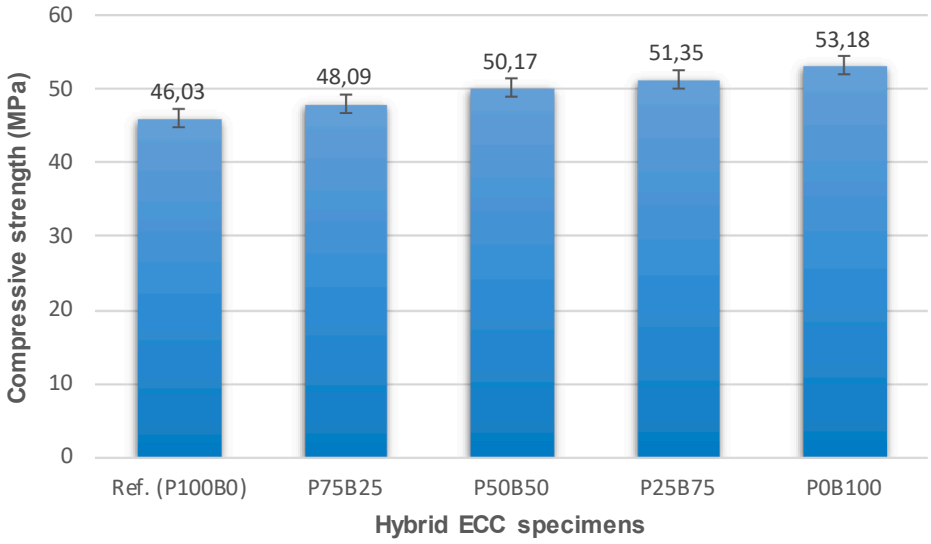


**Fig. 5.** The compressive strength values of HECC samples.

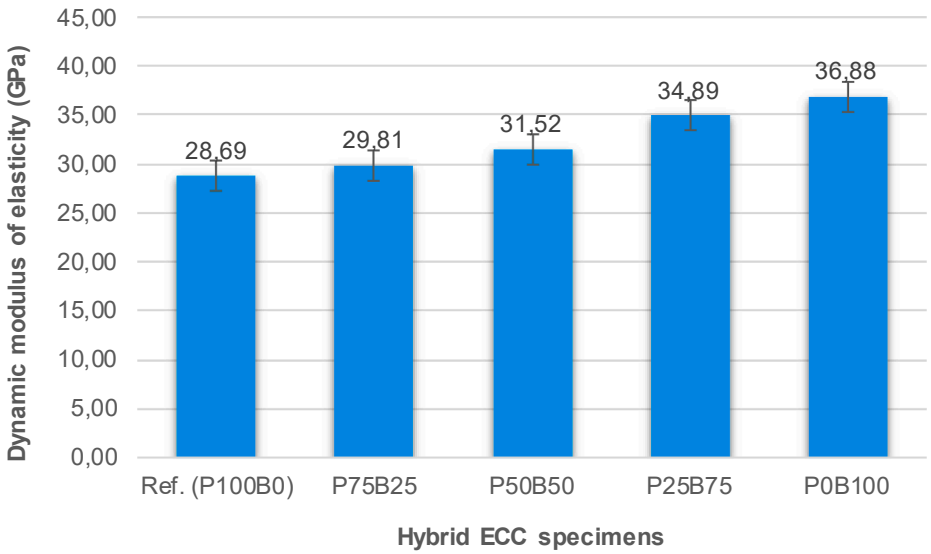


**Fig. 6.** The modulus of elasticity values of HECC samples.

the decrease in the amount of void in the matrix depending on the amount of basalt fiber.

The fibers used in cementitious composite mixtures have a high potential to internally restrain the microstructure of the composite, which increases the toughness and thus contributes to the elasticity of modulus improves the higher elastic modulus values [89]. The high elasticity modulus (89 GPa) of basalt fibers used in hybrid mixtures has increased the modulus of elasticity by improving the toughness of the mixtures [90].

### 3.3. Bulk density

Fig. 7 shows the density of HECC samples. The density of HECC mixtures at the age of 28 days ranges from 1.99 kg/m$^3$ to 2.14 g/cm$^3$. Although these density values are close to the normal concrete value with a typical density of 2.40 g/cm3, it is seen that the densities of all hybrid fiber samples, including the reference sample, are below this value. The minimum density was obtained from P100B0-coded samples (Reference) consisting of 100% PVA fiber of the total fiber content of 2% by volume. The density values of cementitious composite samples are similar to the results obtained in previous studies [15]. It was determined that the density of HECC samples increased as a result of adding basalt fiber. The findings demonstrated that basalt fiber caused an increase in the density of HECC samples with regard to the reference ECC by 0.66%, 3.16%, 6.92% and 7.57% respectively. When compared to the reference samples with 100% PVA fiber, a considerable increase in density occurred as a result of adding basalt fiber. This finding can be associated with the fiber structure of PVA fiber, which has a lower density than basalt fiber (1.3 gr/cm$^3$ and 2.8 gr/cm$^3$, respectively). The less weight of PVA fibers in a certain volume has reduced the density of the mixtures [91]. It was also reported in previous studies that there was an increased density of composites following the incorporation of basalt fiber [92]. Aslan et al. investigated the effect of basalt fiber on the properties of polylactic acid (PLA) composites and found that the material density increased with the increased basalt fiber content [92].

### 3.4. Apparent void volume

Fig. 8 demonstrates the apparent void volume of hybrid composites with different PVA and basalt fiber contents at the age of 28 days.

While a decrease was determined in the apparent void volume of composites with the increasing basalt fiber content, the apparent void volume values of the samples were almost same after 28 days. The reason for this is the fact that the hydration product of the cementitious material fills the voids in composites gradually, which causes an increase in the density and a reduction in the apparent void volume of

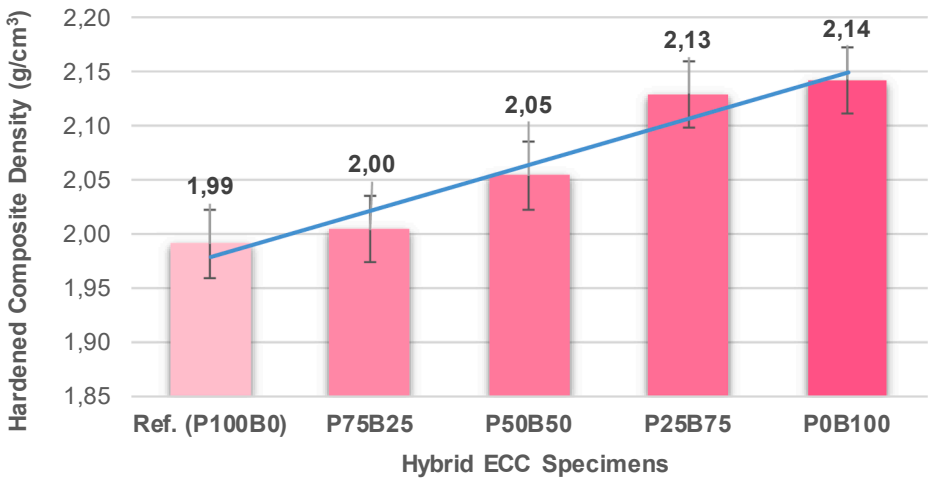


**Fig. 7.** The density of HECC samples.

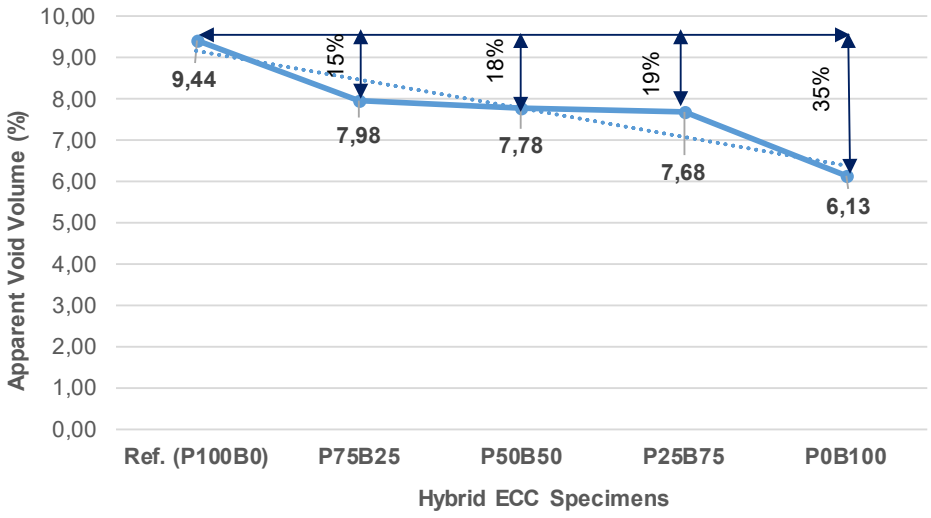


**Fig. 8.** The apparent void volume of hybrid ECC samples.

composites. Another reason for the decrease in the apparent void volume of composites is the decrease in voids due to the homogenous dispersion of hydrophilic basalt fibers in the cementitious matrix.

The apparent void volume of P75B25, P50B50, P25B75, and P0B100 decreased by about 15.46%, 17.60%, 18.73%, and 35.08%, respectively when compared to that of the reference ECC (P100B0). The sample consisting of a combination of 0% PVA and 100% basalt fibers (P0B100) demonstrated the lowest apparent void volume (6.13%) when compared to all other hybrid samples tested at the age of 28 days. The use of a higher dose of basalt fibers in the hybrid ECC mixture (P0B100) decreased the void volume compared to that of P25B75, P50B50 P75B25 and P100B0. As mentioned above, it is possible to attribute this to a more effective spatial distribution of basalt fibers because of fiber features, and the development of the composite density due to the filling role of basalt fiber and the hydration product of cementitious composites. In relation to the development of the composite density, the above-mentioned phenomenon can be attributed to the filling role of the hydration product of cementitious composites as indicated in Section 3.9 SEM analysis.

### 3.5. Water absorption

Fig. 9 demonstrates alterations in the water absorption of composites.

Similar water absorption was obtained in all the composites at the age of 28 days. Nevertheless, there was a slight increase in the water absorption of composites with the decreased basalt fiber content and the increased PVA fiber content in hybrid mixtures. Among all the composites, the hybrid-ECC sample consisting of a combination of 0% PVA and 100% basalt fibers (P0B100) exhibited the minimum increase in water absorption of 6.72% at the age of 28 days. The use of a higher dose of basalt fibers in the ECC mixture (e.g., P25B75 and P0B100) caused a reduction in water absorption.

For instance, the water absorption of samples from mixtures, P75B25, P50B50, P25B75, and P0B100 decreased by about 17.21%, 23.28%, 25.52%, and 44.14% respectively, in comparison with the water absorption of the reference ECC samples containing 2% PVA fiber alone. The slightly higher water absorption of the samples after 28 days of curing is due to the less dense matrix structure caused by the inability of fly ash to fully complete its pozzolanic activity (see Fig. 13). The above-mentioned phenomenon indicates that PVA affects the water

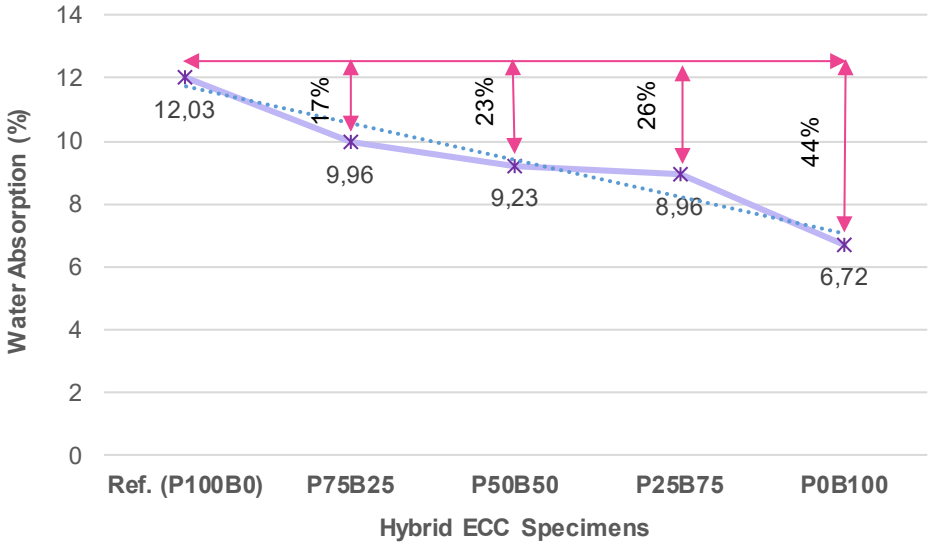


**Fig. 9.** Water absorption of hybrid ECC samples.

absorption of composites, and basalt fiber content is closely associated with the composite density and apparent porosity. Furthermore, this result indicates that the hybridization of PVA and basalt fibers has a superior ability to restrain water absorption in ECC samples.

### 3.6. Capillary water absorption coefficient

The rate of capillary water absorption (sorptivity) is an important parameter that measures the sensitivity to water penetration into cementitious materials. The capillary water absorption test enables the determination of water absorption and transmission tendencies of cementitious samples by capillary action [93]. The low capillary water absorption values obtained as a result of the experimental studies are an indicator of the high material quality due to the low number of pores in the cementitious material. The penetration of water through interconnected pores is a result of internal feature of the cementitious material [94]. In the researches made, capillary water absorption has been accepted as an important indicator in predicting the service life of the material [95,96].

Fig. 10 demonstrates the findings on the average mass variation per contact area in the capillary absorption process for HECCs. The results show that at all minutes of the test, all HECC samples showed minor capillary water absorption compared to the reference sample (P100B0). Generally, these low capillary water absorption values obtained for all mixtures can be attributed to the high content of fly ash and micronized sand, which acts as a filler to compact the microstructure of the composite at an early age [97,98]. At all minutes of the test, the capillary level of P0B100 samples was determined to be lower when compared to other hybrid fiber ECCs.

At the end of the 64th minute, the capillary water absorption of average 0.05 g/($m^2$x$s^{0.5}$) was exhibited by all the composites. Better results in capillary absorption were obtained from P0B100 in comparison with the reference ECC (P100B0). Among the hybrid samples, the highest capillary water absorption was obtained from P75B25 when compared to P50B50, P25B75 and P0B100. The reason for this may be the differences in the compatibility of fibers in addition to variances in water absorption characteristics [99]. Ralegaonkar et al. stated the formation of cracks and its tendency in mortar are decreased by introducing basalt fiber into mortar efficiently which leads to reduced capillary and water penetration of the mortar [100]. The PVA fibers with hydrophobic structure, which are randomly distributed in the matrix and coated with oil, lead to increased porosity in the fiber/matrix interface region of the composite to which they are added, and result in an adverse effect of capillary water absorption [97].

### 3.7. Ultrasonic pulse velocity test (UPV)

In the current experimental study, the ultrasonic pulse velocity (UPV) was utilized for the purpose of monitoring the behaviour of hybrid fiber ECC samples exposed to the water curing regime for 28 days. Fig. 11 presents the ultrasonic pulse velocity result.

In general, higher UPV value indicates that the amount of flaws in the measured composite is less, which accordingly indicates a better composite quality. The UPV results in the current experimental study demonstrate an increment trend in the UPV results of all samples associated with basalt fiber content in hybrid ECC mixtures, and this bears similarity to the trend determined in the bulk density and the Schmidt rebound hammer test. The obtained results demonstrate that all the samples were in the good class of the UPV values classification [101]. At the age of 28 days, the UPV value of all the samples was in the range of 3.76–4.11 km/s of water-cured samples. The classification criterion suggested by Leslie and Cheeseman [101] in Table 5 were used to classify the UPV values of the composite mixtures obtained in this study.

While the highest velocity was determined in sample coded with P0B100, a lower velocity was determined in other hybrid fiber reinforced samples except for sample reinforced by only basalt fiber (P0B100). At the age of 28 days, the UPV of composites decreased slightly with the decreasing basalt fiber content and the increasing PVA fiber content in hybrid mixtures. Among all the composites, reference sample (P100B0) had the lowest UPV value, which was 3.76 km/s. This was 8.51% below the P0B100 coded sample in which the highest value is obtained. The use of a higher dose of basalt fibers in the ECC mixture (e.g., P25B75 and P0B100) increased the UPV. For instance, the ultrasonic pulse velocity of samples from mixtures P75B25, P50B50, P25B75 and P0B100 increased by about 1.60%, 3.19%, %6.65 and 9.31%, respectively, in comparison with the ultrasonic pulse velocity of the reference ECC samples containing 2% PVA fiber alone. The phenomenon in question suggests that the ultrasonic pulse velocity of composites is influenced by PVA and basalt fiber content and is closely related to the composite density and apparent porosity. Moreover, this indicates that including the combination of PVA and basalt fiber has a considerable impact on the cementitious matrix and speeds up the ultrasonic pulse velocity in ECC samples.

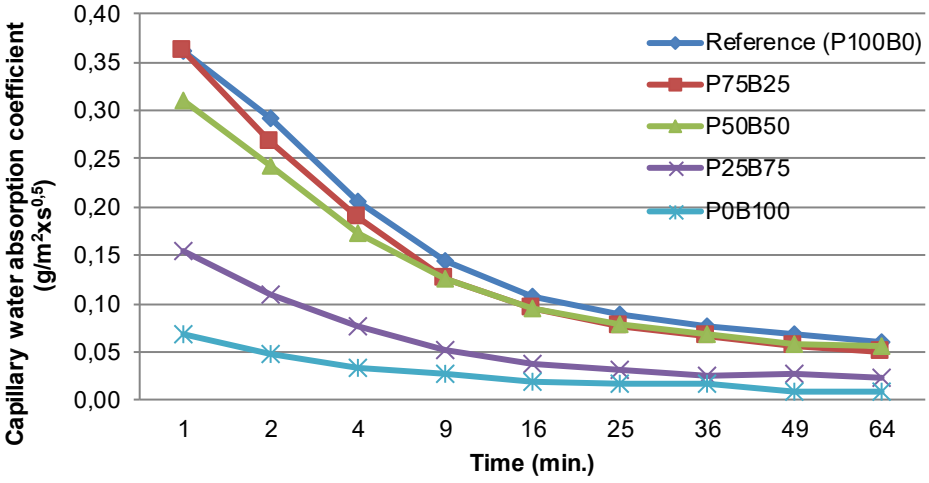


**Fig. 10.** Capillary water absorption curve of hybrid ECC samples as a function of the root of time.

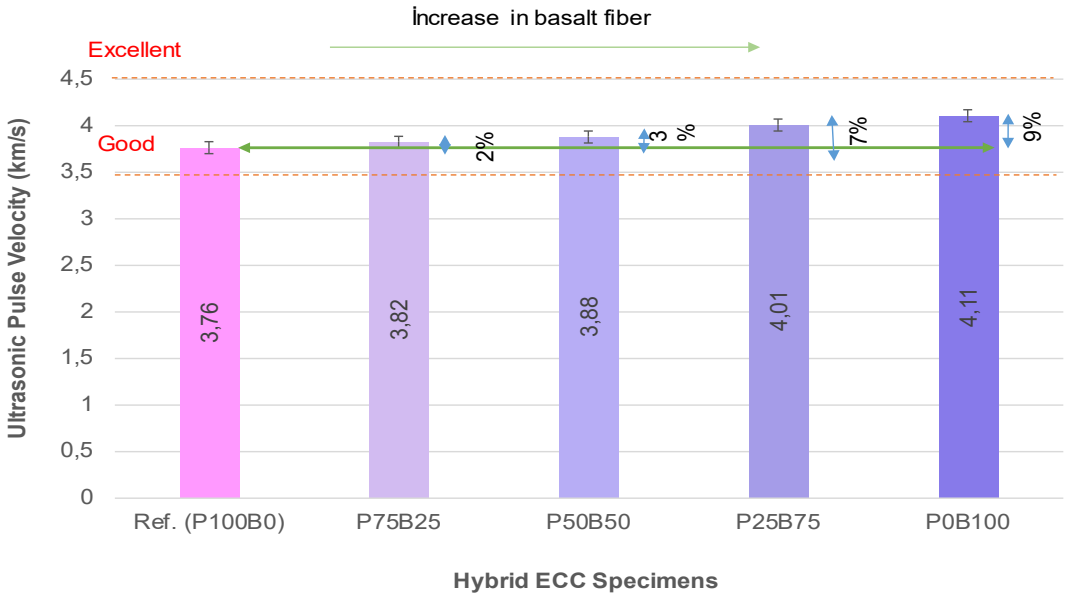


**Fig. 11.** The ultrasonic pulse velocity values of hybrid ECC samples.

**Table 5**
Classification of composites according to ultrasonic pulse velocity test results [101].

| Pulse velocity (km/s) | Concrete classification |
|---|---|
| $V > 4.575$ | Excellent |
| $4.575 > V > 3.660$ | Good |
| $3.660 > V > 3.050$ | Questionable |
| $3.050 > V > 2.135$ | Poor |
| $V < 2.135$ | Very poor |

### 3.8. Schmidt rebound hammer test (SRH)

The rebound hammer test was conducted on samples following 28 days of curing to quantify the impact of fibers on the surface hardness of HECCs. The results of the surface hardness of hybrid ECC mixes with varying percentages of PVA and basalt fiber at 28 days are presented in Fig. 12.

The 28-day results show that the surface hardness values of composites increase slightly with the increasing basalt fiber content and the decreasing PVA fiber content in hybrid mixtures. The surface hardness values of P75B25, P50B50, P25B75, and P0B100 increased by about 12%, 16%, 20% and 28% respectively, in comparison with that of the reference ECC (P100B0). The sample containing 100% basalt fibers (P0B100) demonstrated the highest surface hardness value (32) in comparison with all other tested hybrid samples at the age of 28 days.

As is seen in Fig. 12, including basalt fibers causes an increase in the rebound number of HECCs in comparison with the reference samples. Samples with the hybrid fiber combination have a higher rebound hummer value and higher velocity compared to the reference samples with single fiber (100% PVA fiber). This demonstrates that including PVA fibers decreases the surface hardness and uniformity of HECCs. The above-mentioned impact is observed more in hybrid ECCs with higher PVA fiber content than in hybrid ECCs with higher basalt fiber content. The reason for this may be the uniform distribution of basalt fibers due to the flowable characteristic of ECCs, which causes an increase in the homogeneity and integrity of composites. Another reason for increasing the surface hardness of the composite with the addition of basalt fiber to

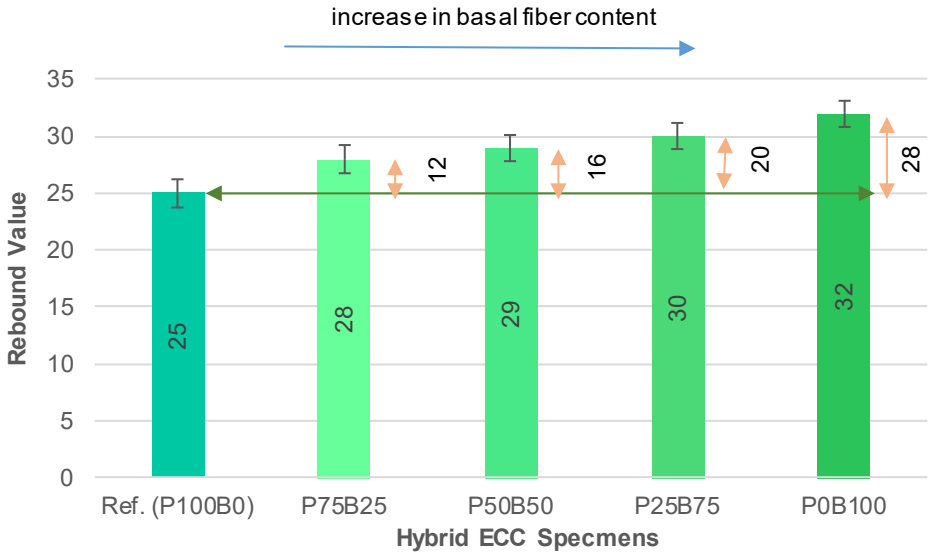


**Fig. 12.** Surface hardness results obtained using a Schmidt hammer.

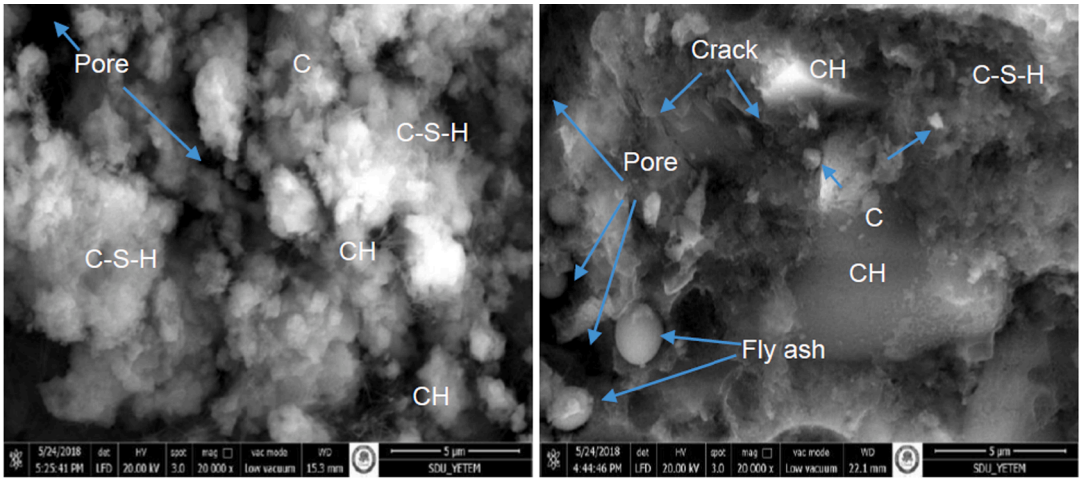


(a) Reference sample (b) P75B25

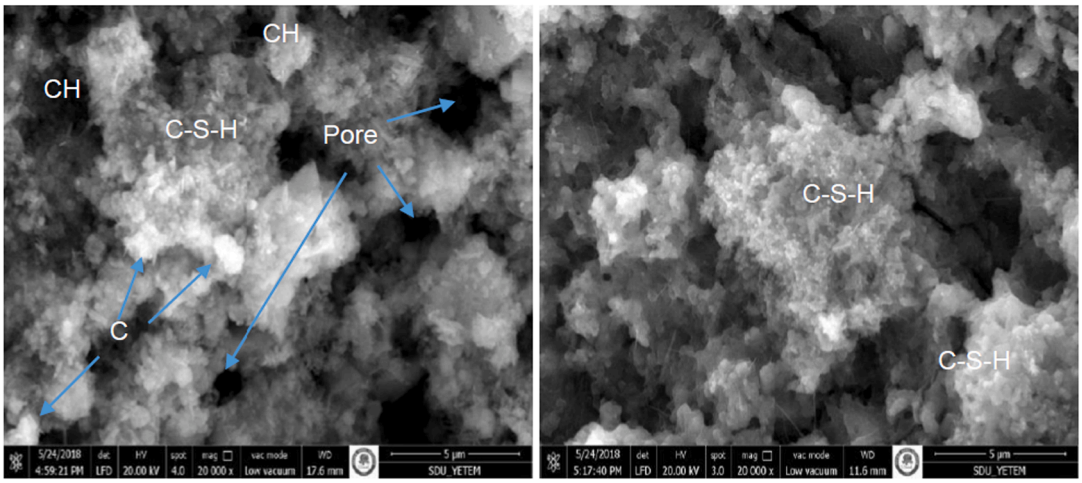


(c) P50B50 (d) P25B75

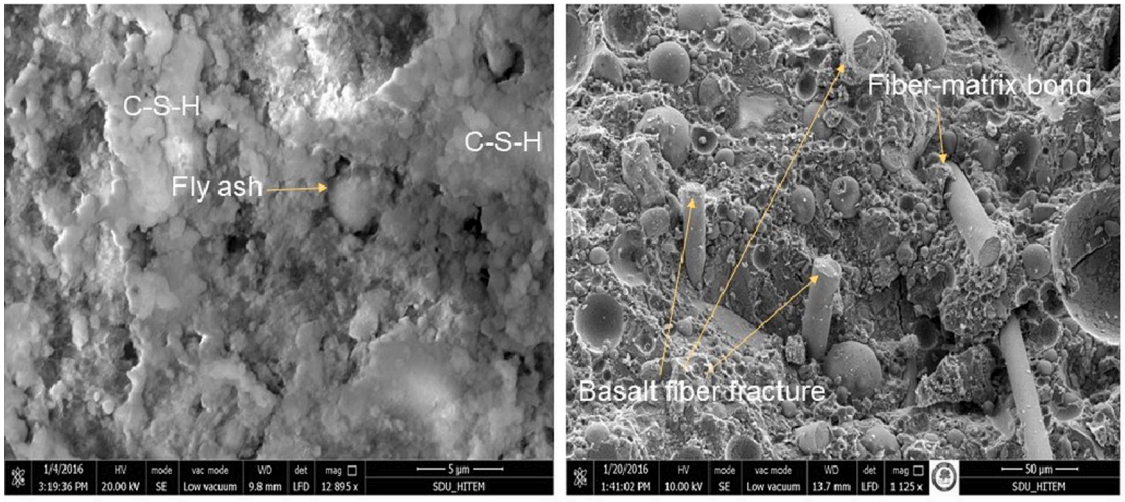


(e) P0B100 (f) fiber fracture resulting from basalt fiber rupture

**Fig. 13.** SEM image of the reference sample, P75B25, P50B50, P25B75 and P0B100 hybrid ECCs at 28 days.

the mixture is thought to be the hydrophilic structure of basalt fiber effecting homogeneous fiber distribution [81–83].

### 3.9. SEM analysis

Fig. 13 demonstrates the scanning electron microscope (SEM) analysis of the reference and hybrid ECCs comprising 100% PVA fiber (Reference), P75B25, P50B50, P25B75 and P0B100. In the SEM image, the formation of calcium silicate hydrate (CSH) and dense structure because of the hydration reaction in the cementitious composite samples are demonstrated. In sample P25B75 and P0B100 (Fig. 13(d), (e)), more CSH and dense structure were determined following 28 days of curing, while a considerable amount of portlandite (CH) was determined in P50B50 and P75B25 HECC samples. Jumate and Manea [102] determined that following 28 days, a mass that demonstrates higher density, higher compactness, and higher continuity is formed by CSH, which causes an increase in strength. Identical observations were performed for hybrid P25B75 and P0B100 (Fig. 13(d), (e)) that exhibited CSH gel formation. Furthermore, calcite (C) was found in all HECC samples, which was responsible for enhanced strength and a decreased pore size in HECCs. A higher number of voids was observed in P50B50 and P75B25 samples in comparison with P25B75 and P0B100 samples with a dense structure. The dense matrix in HECC samples (P25B75 and P0B100) exhibited a higher rebound value, lower water absorption and porosity because of the growth of calcite crystals within the pores of the cement-sand matrix [103]. In a number of cases, pores were determined between fibers and the matrix, but it was thought to be the outcome of mechanical deterioration because of testing or sample preparation. Fig. 13(e) shows the dense and rough structure of the matrix, which contributes to more advanced physical bonding and lower moisture transfer [104]. Strong adhesion between fiber and matrix causes fibers to fracture [74]. This strong bonding formed by matrix and basalt fiber was sufficient to create fiber fracture behavior, which contributed to reduced water permeation and matrix porosity (Fig. 13(f)) [104].

### 3.10. Correlations between the physical properties of hybrid fiber reinforced cementitious composites

In this section, the relationship between the densities of cementitious composites and other parameters is examined. When the graphic in Fig. 14 is examined, a linear behavior tendency of approximately 94% is observed between the increase of basalt fiber content and the density of hardened cementitious composites.

When the graphic in Fig. 14 is analyzed, the correlation coefficient ($R^2$) was found as 0.943. The obtained value indicates that there is a good relationship between the above two parameters The relationship between density versus basalt fiber content in Fig. 14 reveals that the density increases depending on the increase in fiber content or vice versa.

The most appropriate model, which explains the relationship between density and apparent void volume values and is also compatible with the literature [105], is the linear function relationship model. Therefore, a linear relationship model was used. The correlation between dry density and apparent void volume values of composite mixtures obtained from experimental data is shown in Fig. 15. When the graph is examined, the equation $y = -0{,}0484x + 2{,}4396$ indicates that there is an inversely correlated relationship between density and apparent void volume variables. Finding the correlation coefficient as $R^2 = 0.651$ indicates that there is a moderate positive relationship between the two variables. The density versus apparent void volume relationship reveals that the decrease in void volume is effective in increasing density or vice versa.

The correlation between dry density and water absorption values of composite mixtures obtained from experimental data is shown in Fig. 16. When the graph is examined, the equation $y = -23{,}189x + 57{,}196$ indicates that there is a linear relationship between density and water absorption variables. Finding the correlation coefficient as $R^2 = 0.7305$ indicates that there is a moderate positive relationship between the two variables. The relationship between density and water absorption reveals that the decrease in density is effective in increasing water absorption and vice versa.

From these results, it can be argued that the densities of hybrid fiber reinforced cementitious composites was affected by apparent void volume and water absorption percentages. Therefore, the increase in the density of cementitious composites along with the increase in the amount of basalt fiber in hybrid fiber content had a positive effect on physical and durability properties such as void volume, water absorption percent by weight, and capillary water absorption (sorptivity).

### 3.11. Correlation between compressive strength and non-destructive tests

Correlation analysis was conducted to determine the relationship between compressive strength and SRH and UPV at 28 days. Compressive strength, SRH and UPV test results were used to create the correlation curves. As can be seen in Fig. 17, the compressive strength values vary in direct proportion to the SRH and UPV values.

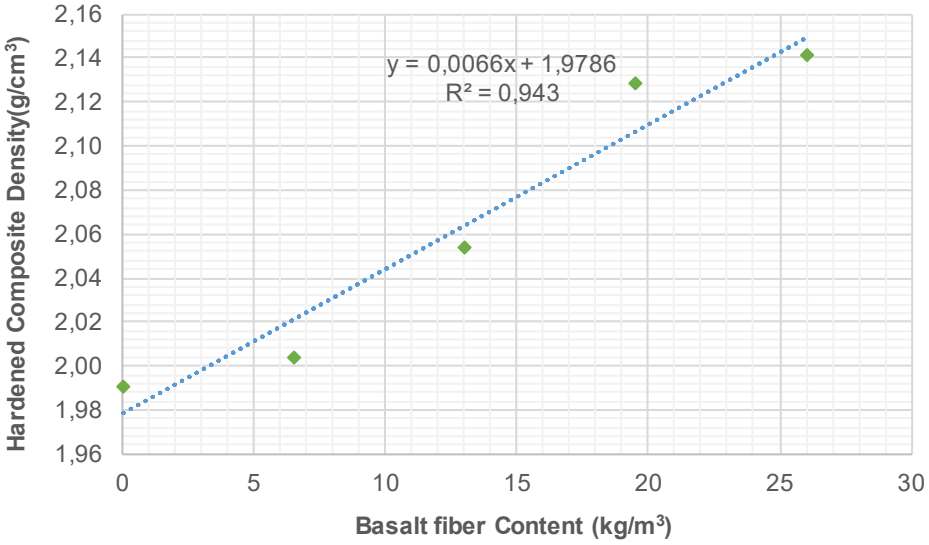


**Fig. 14.** The relationship between hardened composite density and fiber content.

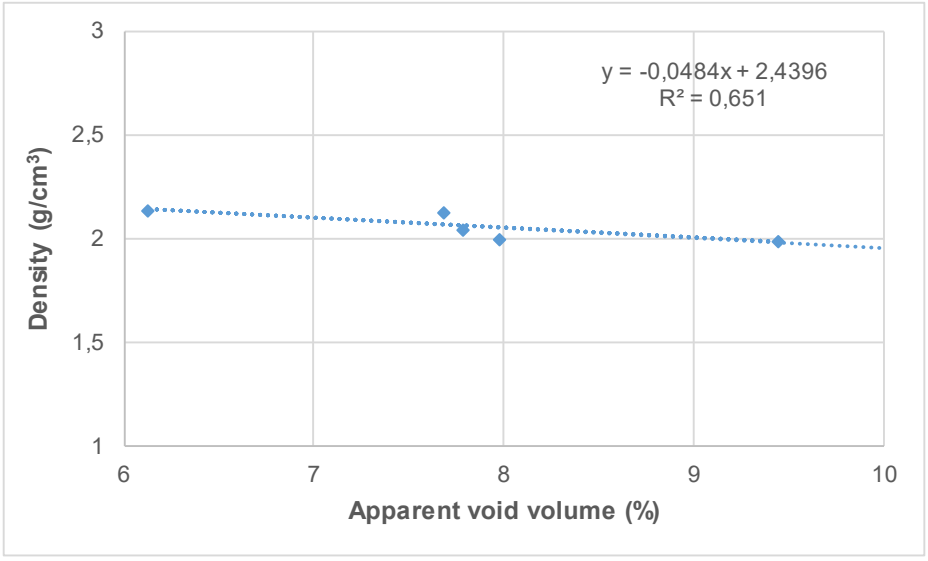


**Fig. 15.** The relationship between density and apparent void volume.

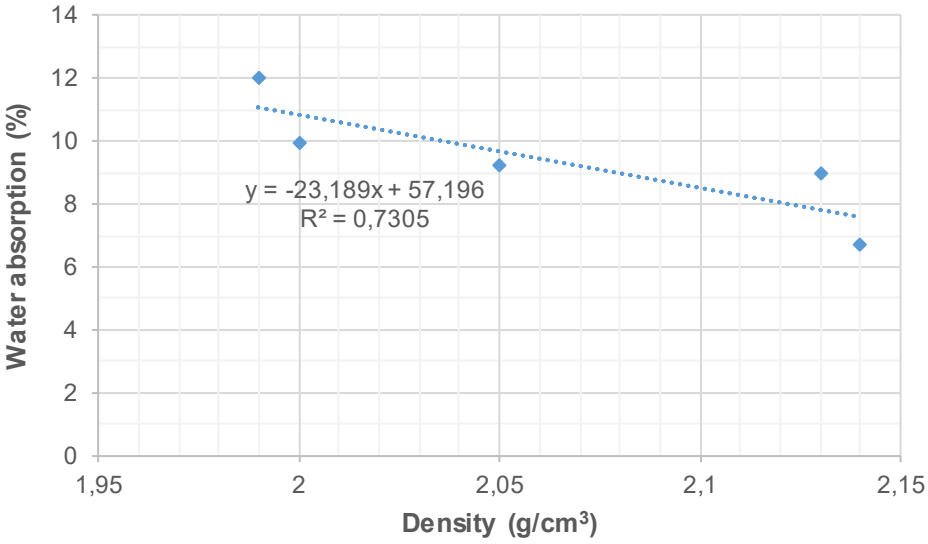


**Fig. 16.** The relationship between density and water absorption.

The best fit line expressing the relationship between compressive strength and UPV is presented in Fig. 17 by performing regression analysis. As a result of the analysis, a linear equation (Eq. (7)) y = 18.942x-24.414, which indicates a linear relationship between the two properties, was obtained.

$$y = 18.942x - 24.414 \quad (7)$$

where, y and x represent 28 days compressive strength (MPa) and ultrasonic pulse velocity (km/s), respectively.

Fig. 17 also shows that the best fit line expressing the relationship between 28 days compressive strength and RN is found as in the following equation (Eq. (8)) as a result of the analysis.

$$y = 1.0613x + 19.197 \quad (8)$$

where y and x represent 28 days compressive strength (MPa) and rebound number, respectively. The R squared value was found to be 0.97.

The equation clearly shows that the compressive strength and RN vary linearly. The fact that the regression analysis coefficient is equal to 0.9941 shows that there is a good relationship between the compressive strength and RN.

*3.11.1. Models for compressive strength versus UPV and RN*

Two linear models showing the relationship between compressive strength-UPV and compressive strength-RN are shown graphically in Fig. 17 and regression results are given in Table 6.

The obtained high coefficient ($R^2$ = 0.94) shows that there is an excellent correlation between compressive strength and UPV at 28 days. Therefore, it can be interpreted that the regression model explains about 94% of the total variance in UPV. The p-values for the intercept and UPV variable were found as 0.0082 and 0.0021 (<0.05), respectively. These values indicate that the results are reliable (statistically significant), the UPV variable is important in terms of its contribution to the model, and the variable should be retained in the model. As a result, it can be said that the model developed based on experimental data is sufficient in explaining the data.

Table 6 presents the variance analysis (ANOVA) conducted to determine the compressive strength-UPV relationship. As seen, the F test value showing the significance of entire model was found as $F_0$ =

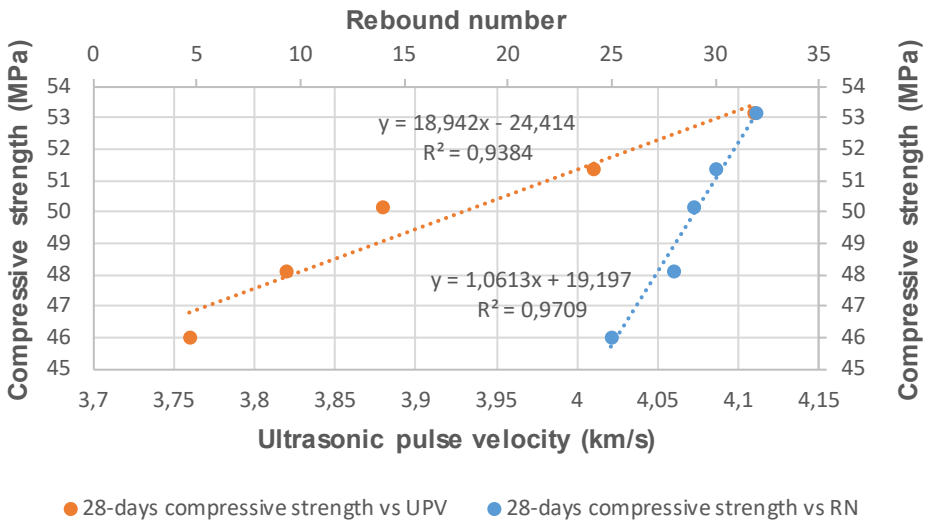


**Fig. 17.** Relationship between compressive strength with UPV and rebound number for hybrid fiber reinforced cementitious composites at the age of 28 days.

**Table 6**
Regression output for compressive strength versus non-destructive test data.

| Age (days) | Relationship | $R^2$ | Adjust $R^2$ | $F_0$ | Significance of regression | *p*-Value | |
|---|---|---|---|---|---|---|---|
| | | | | | | Intercept | Variable |
| 28 | Compressive strength versus UPV | 0.97 | 0.99 | 100.02 | 0.00212 | 0.0082 | 0.0021 |
| | Compressive strength versus RN | 0.94 | 0.92 | 45.68 | 0.00661 | 0.11 | 0.0066 |

100.02. In addition, the p value was obtained as 0.0021. Since this value is less than the critical values (10% and 5%), the zero hypothesis (i.e. that the coefficients of the variables in the model should be zero) is rejected and the alternative hypothesis is accepted (i.e. that the parameters in the model are not zero and the contribution of the term to the hypothesis is important). Therefore, the model, where the dependent variable is strength and the independent variable is UPV, is significant ($p < .05$).

In the results of the analysis of variance (ANOVA) conducted to determine the compressive strength-RN relationship, it is seen that the obtained p value (0.00661) indicating the significance of the regression is smaller than the critical values. Therefore, the interpretations made for the compressive strength-UPV relationship can also be made for the compressive strength-RN relationship.

## 4. Conclusions

The current study encompasses the experimental investigation of the properties of hybrid engineered cementitious composites reinforced with basalt fibers in combination with PVA fiber comprising the high volume of fly ash. The main conclusions obtained in the study are presented as follows:

The performance of engineered cementitious composite samples with hybrid PVA and basalt fiber reinforcement was evaluated by conducting bulk density, apparent void volume, water absorption, capillary water absorption, and non-destructive tests (including ultrasonic pulse velocity and the Schmidt rebound hammer test). It is possible to draw the following conclusions on the basis of the experimental findings:

- An increase in the basalt fiber content and the decrease in the PVA fiber content in hybrid ECC mixtures led to slight increase in the bulk density, decrease in the apparent void volume (porosity), water absorption, and capillary water absorption.
- The experimental results demonstrated that the HECC mix containing only 100% basalt fiber (P0B100) reduced void volume by 35.08% in comparison with the control sample (P100B0), which had a 9.44% value.
- The highest UPV values were obtained from P0B100 samples with the highest Schmidt rebound hammer value. Also, a close association between UPV and density was determined in the overall HECC samples.
- The highest capillary water absorption coefficient value was obtained from Reference (P100B0) and P75B25 samples, which had the lowest Schmidt rebound hammer values compared to those of the other tested samples (P50B50, P25B75 and P0B100). However, the lowest capillary water absorption coefficient value was obtained from P0B100 sample that performed the best in the Schmidt rebound hammer test.
- Experimental results demonstrated that the hybridization mechanism of PVA fiber with basalt fiber led to a slower water absorption process. In general, hybridization of PVA with basalt fiber in HECCs has been found to improve the mechanical and physical properties of composites, which is thought to expand the potential application of this cementitious material.
- In terms of some properties, basalt fiber has superior structural properties compared to PVA fiber, so both mechanical and physical properties of P0B100-coded HECC were superior to those of other hybrid samples due to incorporating of more basalt fiber in the composite mixture.

In conclusion, the current study showed that hybridization with fibers with various physical, durability and mechanical characteristics might be very efficient in improving the qualities of HECC materials considerably. Furthermore, it will be useful to study the impact of various fiber types and mixture proportions on the physical and mechanical characteristics of HECCs.

*CRediT authorship contribution statement*

**Şükrü Özkan:** Conceptualization, Methodology, Formal analysis,

Investigation, Resources, Writing – original draft, Writing – review & editing, Project administration, Visualization. **Ömer Çoban:** Conceptualization, Methodology, Writing – review & editing.

## Declaration of Competing Interest

The authors declare that they have no known competing financial interests or personal relationships that could have appeared to influence the work reported in this paper.

## Acknowledgments

The authors would like to thank Spinteks, the Turkey distributor of Technobasalt-Invest LLC, for supplying basalt fiber and sharing technical information.

## References

[1] W.-J. Long, H.-D. Li, L. Mei, W. Li, F. Xing, K.H. Khayat, Damping characteristics of PVA fiber-reinforced cementitious composite containing high-volume fly ash under frequency-temperature coupling effects, Cem. Concr. Compos. 118 (2021) 103911, https://doi.org/10.1016/j.cemconcomp.2020.103911.

[2] J.-X. Lin, Y. Song, Z.-H. Xie, Y.-C. Guo, B. Yuan, J.-J. Zeng, X. Wei, Static and dynamic mechanical behavior of engineered cementitious composites with PP and PVA fibers, J. Build. Eng. 29 (2020) 101097, https://doi.org/10.1016/j.jobe.2019.101097.

[3] Q. Wang, M.H. Lai, J. Zhang, Z. Wang, J.C.M. Ho, Greener engineered cementitious composite (ECC) – The use of pozzolanic fillers and unoiled PVA fibers, Constr. Build. Mater. 247 (2020) 118211, https://doi.org/10.1016/j.conbuildmat.2020.118211.

[4] Q.-H. Li, C.-J. Sun, S.-L. Xu, Thermal and mechanical properties of ultrahigh toughness cementitious composite with hybrid PVA and steel fibers at elevated temperatures, Compos. B Eng. 176 (2019) 107201, https://doi.org/10.1016/j.compositesb.2019.107201.

[5] A. Dehghani, F. Aslani, The synergistic effects of shape memory alloy, steel, and carbon fibres with polyvinyl alcohol fibres in hybrid strain-hardening cementitious composites, Constr. Build. Mater. 252 (2020) 119061, https://doi.org/10.1016/j.conbuildmat.2020.119061.

[6] M. Xu, S. Song, L. Feng, J. Zhou, H. Li, V.C. Li, Development of basalt fiber engineered cementitious composites and its mechanical properties, Constr. Build. Mater. 266 (2021) 121173, https://doi.org/10.1016/j.conbuildmat.2020.121173.

[7] J.-H. Kim, C.-G. Park, S.-W. Lee, S.-W. Lee, J.-P. Won, Effects of the geometry of recycled PET fiber reinforcement on shrinkage cracking of cement-based composites, Compos. B Eng. 39 (3) (2008) 442–450, https://doi.org/10.1016/j.compositesb.2007.05.001.

[8] J. Yu, J. Yao, X. Lin, H. Li, J.Y.K. Lam, C.K.Y. Leung, I.M.L. Sham, K. Shih, Tensile performance of sustainable strain-hardening cementitious composites with hybrid PVA and recycled PET fibers, Cem. Concr. Res. 107 (2018) 110–123, https://doi.org/10.1016/j.cemconres.2018.02.013.

[9] V. Fiore, T. Scalici, G. Di Bella, A. Valenza, A review on basalt fibre and its composites, Compos. B Eng. 74 (2015) 74–94, https://doi.org/10.1016/j.compositesb.2014.12.034.

[10] X. Lin, J. Yu, H. Li, J.Y.K. Lam, K. Shih, I.M.L. Sham, C.K.Y. Leung, Recycling polyethylene terephthalate wastes as short fibers in Strain-Hardening Cementitious Composites (SHCC), J. Hazard. Mater. 357 (2018) 40–52, https://doi.org/10.1016/j.jhazmat.2018.05.046.

[11] M.J. Chinchillas-Chinchillas, A. Gaxiola, C.G. Alvarado-Beltrán, V.M. Orozco-Carmona, M.J. Pellegrini-Cervantes, M. Rodríguez-Rodríguez, A. Castro-Beltrán, A new application of recycled-PET/PAN composite nanofibers to cement–based materials, J. Cleaner Prod. 252 (2020) 119827, https://doi.org/10.1016/j.jclepro.2019.119827.

[12] D. Wang, Y. Ju, H. Shen, L. Xu, Mechanical properties of high performance concrete reinforced with basalt fiber and polypropylene fiber, Constr. Build. Mater. 197 (2019) 464–473, https://doi.org/10.1016/j.conbuildmat.2018.11.181.

[13] G. Yıldırım, M. Şahmaran, Ö. Anıl, in: Eco-Efficient Repair and Rehabilitation of Concrete Infrastructures, Elsevier, 2018, pp. 387–427, https://doi.org/10.1016/B978-0-08-102181-1.00015-0.

[14] M. Lepech, V.L.-P. of the I.W. on, undefined 2005, Durability and long term performance of engineered cementitious composites, Academia.Edu. (2007). https://www.academia.edu/download/46335465/Long_Term_Durability_Performance_of_Engi20160608-12610-598bj1.pdf (accessed September 21, 2021).

[15] V.C. Li, Engineered Cementitious Composites (ECC)-Material, Structural, and Durability Performance, 2007. https://deepblue.lib.umich.edu/bitstream/handle/2027.42/84661/ECC_Book_Chapter.pdf?sequence=1 (accessed April 23, 2021).

[16] P. Zhang, K. Wang, J. Wang, J. Guo, S. Hu, Y. Ling, Mechanical properties and prediction of fracture parameters of geopolymer/alkali-activated mortar modified with PVA fiber and nano-SiO2, Ceram. Int. 46 (12) (2020) 20027–20037, https://doi.org/10.1016/j.ceramint.2020.05.074.

[17] A. Mohammedameen, M.E. Gülşan, R. Alzeebaree, A. Çevik, A. Niş, Mechanical and durability performance of FRP confined and unconfined strain hardening cementitious composites exposed to sulfate attack, Constr. Build. Mater. 207 (2019) 158–173, https://doi.org/10.1016/J.CONBUILDMAT.2019.02.108.

[18] Y. Zheng, P. Zhang, Y. Cai, Z. Jin, E. Moshtagh, Cracking resistance and mechanical properties of basalt fibers reinforced cement-stabilized macadam, Compos. B Eng. 165 (2019) 312–334, https://doi.org/10.1016/J.COMPOSITESB.2018.11.115.

[19] N. Kabay, Abrasion resistance and fracture energy of concretes with basalt fiber, Constr. Build. Mater. 50 (2014) 95–101, https://doi.org/10.1016/j.conbuildmat.2013.09.040.

[20] C. Jiang, S. Huang, Y. Zhu, Y. Lin, D.a. Chen, Effect of polypropylene and basalt fiber on the behavior of mortars for repair applications, Adv. Mater. Sci. Eng. 2016 (2016) 1–11, https://doi.org/10.1155/2016/5927609.

[21] H.R. Pakravan, M. Jamshidi, A.A. Asgharian Jeddi, Combination of ground rice husk and polyvinyl alcohol fiber in cementitious composite, J. Environ. Manage. 215 (2018) 116–122, https://doi.org/10.1016/j.jenvman.2018.03.035.

[22] R.S. Teixeira, S.F. Santos, A.L. Christoforo, J. Payá, H. Savastano, F.A.R. Lahr, Impact of content and length of curauá fibers on mechanical behavior of extruded cementitious composites: analysis of variance, Cem. Concr. Compos. 102 (2019) 134–144, https://doi.org/10.1016/j.cemconcomp.2019.04.022.

[23] X. Shang, J. Yang, Q. Song, L. Wang, Efficacy of modified rice straw fibre on properties of cementitious composites, J. Cleaner Prod. 276 (2020) 124184, https://doi.org/10.1016/j.jclepro.2020.124184.

[24] P. Júnior Carvalho Machado, R. Alberto dos Reis Ferreira, L. Aparecida de Castro Motta, D. Pasquini, Characterization and properties of cementitious composites with cellulose fiber, silica fume and latex, Constr. Build. Mater. 257 (2020) 119602, https://doi.org/10.1016/j.conbuildmat.2020.119602.

[25] Z. Wang, K. Zhao, Z. Li, H. Ma, Experimental study on durability and mechanical properties of basalt fiber reinforced concrete under sodium sulfate erosion, Chem. Eng. Trans. 62 (2017) 961–966, https://doi.org/10.3303/CET1762161.

[26] M. Şahmaran, V.C. Li, Durability properties of micro-cracked ECC containing high volumes fly ash, Cem. Concr. Res. 39 (11) (2009) 1033–1043, https://doi.org/10.1016/j.cemconres.2009.07.009.

[27] M. Hanafi, E. Aydin, A. Ekinci, Engineering properties of basalt fiber-reinforced bottom ash cement paste composites, Materials 13 (2020) 1952, https://doi.org/10.3390/ma13081952.

[28] N. Azlina Ramlee, M. Jawaid, S. Abdul Karim Yamani, E. Syams Zainudin, S. Alamery, Effect of surface treatment on mechanical, physical and morphological properties of oil palm/bagasse fiber reinforced phenolic hybrid composites for wall thermal insulation application, Constr. Build. Mater. 276 (2021) 122239, https://doi.org/10.1016/j.conbuildmat.2020.122239.

[29] C.V. Nguyen, P.S. Mangat, Properties of rice straw reinforced alkali activated cementitious composites, Constr. Build. Mater. 261 (2020) 120536, https://doi.org/10.1016/j.conbuildmat.2020.120536.

[30] A. Noushini, B. Samali, K. Vessalas, Effect of polyvinyl alcohol (PVA) fibre on dynamic and material properties of fibre reinforced concrete, Constr. Build. Mater. 49 (2013) 374–383, https://doi.org/10.1016/j.conbuildmat.2013.08.035.

[31] Z. Lafhaj, M. Goueygou, A. Djerbi, M. Kaczmarek, Correlation between porosity, permeability and ultrasonic parameters of mortar with variable water/cement ratio and water content, Cem. Concr. Res. 36 (4) (2006) 625–633, https://doi.org/10.1016/j.cemconres.2005.11.009.

[32] A.M.T. Hassan, S.W. Jones, Non-destructive testing of ultra high performance fibre reinforced concrete (UHPFRC): A feasibility study for using ultrasonic and resonant frequency testing techniques, Constr. Build. Mater. 35 (2012) 361–367, https://doi.org/10.1016/j.conbuildmat.2012.04.047.

[33] L. Li, M. Cao, Influence of calcium carbonate whisker and polyvinyl alcohol- steel hybrid fiber on ultrasonic velocity and resonant frequency of cementitious composites, Constr. Build. Mater. 188 (2018) 737–746, https://doi.org/10.1016/j.conbuildmat.2018.08.154.

[34] Y.u. Zhu, Z. Zhang, X.u. Chen, D. Zou, X. Guan, B. Dong, Non-destructive methods to evaluate the self-healing behavior of engineered cementitious composites (ECC), Constr. Build. Mater. 230 (2020) 116753, https://doi.org/10.1016/j.conbuildmat.2019.116753.

[35] VM Malhotra, N.J. Carino. Handbook on nondestructive testing of concrete, CRC press, 2003.

[36] S.P. Yap, U.J. Alengaram, M.Z. Jumaat, Enhancement of mechanical properties in polypropylene- and nylon-fibre reinforced oil palm shell concrete, Mater. Des. 49 (2013) 1034–1041, https://doi.org/10.1016/j.matdes.2013.02.070.

[37] A. Sadeghi Nik, O. Lotfi Omran, Estimation of compressive strength of self-compacted concrete with fibers consisting nano-SiO2 using ultrasonic pulse velocity, Constr. Build. Mater. 44 (2013) 654–662, https://doi.org/10.1016/j.conbuildmat.2013.03.082.

[38] S.R. Mishra, S. Kumar, A. Park, J. Rho, J. Losby, B.K. Hoffmeister, Ultrasonic characterization of the curing process of PCC fly ash-cement composites, Mater. Charact. 50 (4-5) (2003) 317–323, https://doi.org/10.1016/S1044-5803(03)00127-X.

[39] S.L. Suhaendi, T. Horiguchi, Effect of short fibers on residual permeability and mechanical properties of hybrid fibre reinforced high strength concrete after heat exposition, Cem. Concr. Res. 36 (9) (2006) 1672–1678, https://doi.org/10.1016/j.cemconres.2006.05.006.

[40] M. Tabatabaeian, A. Khaloo, A. Joshaghani, E. Hajibandeh, Experimental investigation on effects of hybrid fibers on rheological, mechanical, and durability properties of high-strength SCC, Constr. Build. Mater. 147 (2017) 497–509, https://doi.org/10.1016/j.conbuildmat.2017.04.181.

[41] A. Prakash, S.M. Srinivasan, A. Rama Mohan Rao, Application of steel fibre reinforced cementitious composites in high velocity impact resistance, Mater. Struct./Mater. Constr. 50 (2017) 1–16, https://doi.org/10.1617/s11527-016-0872-y.
[42] M. Alwash, D. Breysse, Z.M. Sbartaï, Non-destructive strength evaluation of concrete: analysis of some key factors using synthetic simulations, Constr. Build. Mater. 99 (2015) 235–245, https://doi.org/10.1016/j.conbuildmat.2015.09.023.
[43] K. Amini, M. Jalalpour, N. Delatte, Advancing concrete strength prediction using non-destructive testing: Development and verification of a generalizable model, Constr. Build. Mater. 102 (2016) 762–768, https://doi.org/10.1016/j.conbuildmat.2015.10.131.
[44] Ş. Karahan, A. Büyüksaraç, E. Işık, The relationship between concrete strengths obtained by destructive and non-destructive methods, iranian journal of science and technology, Trans. Civ. Eng. 44 (2020) 91–105, https://doi.org/10.1007/s40996-019-00334-3.
[45] H.Y. Qasrawi, Concrete strength by combined nondestructive methods simply and reliably predicted, Cem. Concr. Res. 30 (5) (2000) 739–746, https://doi.org/10.1016/S0008-8846(00)00226-X.
[46] Y.N. Sheen, D.H. Le, T.H. Sun, Innovative usages of stainless steel slags in developing self-compacting concrete, Constr. Build. Mater. 101 (2015) 268–276, https://doi.org/10.1016/j.conbuildmat.2015.10.079.
[47] A. El Mir, S.G. Nehme, Repeatability of the rebound surface hardness of concrete with alteration of concrete parameters, Constr. Build. Mater. 131 (2017) 317–326, https://doi.org/10.1016/j.conbuildmat.2016.11.085.
[48] J.-K. Kim, C.-Y. Kim, S.-T. Yi, Y. Lee, Effect of carbonation on the rebound number and compressive strength of concrete, Cem. Concr. Compos. 31 (2) (2009) 139–144, https://doi.org/10.1016/j.cemconcomp.2008.10.001.
[49] C.V. Silva, J.E. Zorzi, R.C.D. Cruz, D.C.C. Dal Molin, Experimental evidence that micro and macrostructural surface properties markedly influence on abrasion resistance of concretes, Wear 422–423 (2019) 191–200, https://doi.org/10.1016/j.wear.2019.01.063.
[50] I. Tekin, M. Yasin Durgun, O. Gencel, T. Bilir, W. Brostow, H.E. Hagg Lobland, Concretes with synthetic aggregates for sustainability, Constr. Build. Mater. 133 (2017) 425–432, https://doi.org/10.1016/j.conbuildmat.2016.12.110.
[51] H.P. Satpathy, S.K. Patel, A.N. Nayak, Development of sustainable lightweight concrete using fly ash cenosphere and sintered fly ash aggregate, Constr. Build. Mater. 202 (2019) 636–655, https://doi.org/10.1016/j.conbuildmat.2019.01.034.
[52] M. Kazemi, R. Madandoust, J. de Brito, Compressive strength assessment of recycled aggregate concrete using Schmidt rebound hammer and core testing, Constr. Build. Mater. 224 (2019) 630–638, https://doi.org/10.1016/j.conbuildmat.2019.07.110.
[53] B.S. Mohammed, Z.I. Syed, V. Khed, M.S. Qasim, Evaluation of nano-silica modified ECC Based on ultrasonic pulse velocity and rebound hammer, Open Civ. Eng. J. 11 (1) (2017) 638–649, https://doi.org/10.2174/1874149501711010638.
[54] B.S. Mohammed, N.J. Azmi, M. Abdullahi, Evaluation of rubbercrete based on ultrasonic pulse velocity and rebound hammer tests, Constr. Build. Mater. 25 (3) (2011) 1388–1397, https://doi.org/10.1016/j.conbuildmat.2010.09.004.
[55] T.H. Panzera, J.C. Rubio, C.R. Bowen, W.L. Vasconcelos, K. Strecker, Correlation between structure and pulse velocity of cementitious composites, Adv. Cem. Res. 20 (3) (2008) 101–108, https://doi.org/10.1680/adcr.2008.20.3.101.
[56] S. Wang, V.L.- Proc., I.W. on H. Structural, undefined 2005, Polyvinyl alcohol fiber reinforced engineered cementitious composites: material design and performances, Citeseer. (n.d.). http://citeseerx.ist.psu.edu/viewdoc/download?doi=10.1.1.67.4523&rep=rep1&type=pdf (accessed October 1, 2021).
[57] Advances in Composite Materials: Analysis of Natural and Man-Made Materials - Google Kitaplar, (n.d.). https://books.google.com.tr/books?hl=tr&lr=&id=PdCPDwAAQBAJ&oi=fnd&pg=PA411&dq=Ultrasonic+pulse+velocity+evaluation+of+cementitious+materials&ots=V9eC6p7rAK&sig=h6DpCZnuB-4O7ILpmdfpCvcBNJI&redir_esc=y#v=onepage&q=Ultrasonic pulse velocity evaluation of cementitious materials&f=false (accessed October 1, 2021).
[58] S. Krishna Rao, P. Sravana, T. Chandrasekhara Rao, Experimental studies in ultrasonic pulse velocity of roller compacted concrete pavement containing fly ash and M-sand studies in ultrasonic pulse velocity of roller compacted concrete pavement, Int. J. Pavement Res. Technol. 9 (4) (2016) 289–301, https://doi.org/10.1016/j.ijprt.2016.08.003.
[59] Z.M. Sbartaï, S. Laurens, S.M. Elachachi, C. Payan, Concrete properties evaluation by statistical fusion of NDT techniques, Constr. Build. Mater. 37 (2012) 943–950, https://doi.org/10.1016/j.conbuildmat.2012.09.064.
[60] Şükrü Özkan, F. Demir, The hybrid effects of PVA fiber and basalt fiber on mechanical performance of cost effective hybrid cementitious composites, Constr. Build. Mater. 263 (2020) 120564, https://doi.org/10.1016/j.conbuildmat.2020.120564.
[61] Q. Wang, Y. Yi, G. Ma, H. Luo, Hybrid effects of steel fibers, basalt fibers and calcium sulfate on mechanical performance of PVA-ECC containing high-volume fly ash, Cem. Concr. Compos. 97 (2019) 357–368, https://doi.org/10.1016/j.cemconcomp.2019.01.009.
[62] Z.P. Loh, K.H. Mo, C.G. Tan, S.H. Yeo, Mechanical characteristics and flexural behaviour of fibre-reinforced cementitious composite containing pva and basalt fibres, Sadhana – Acad. Proc. Eng. Sci. 44 (2019) 1–9, https://doi.org/10.1007/s12046-019-1072-6.
[63] ASTM C150/C150M–20, Standard specification for Portland cement 2020 West Conshohocken, Philadelphia 10.1520/C0150_C0150M-20.
[64] A. C618-19, Standard Specification for Coal Fly Ash and Raw or Calcined Natural Pozzolan for Use, West Conshohocken, Philadelphia, 2019. https://doi.org/10.1520/C0618-19.
[65] A.C., C494M–19, Standard Specification for Chemical Admixtures for Concrete 2019 West Conshohocken, Philadelphia.
[66] S. Wang, Tensile strain-hardening behavior of polyvinyl alcohol engineered cementitious composite (PVA-ECC), Mater. J. 98 (2001) 483–492, https://doi.org/10.14359/10851.
[67] A.C./ C192M-19, Standard Practice for Making and Curing Concrete Test Specimens in the Laboratory, West Conshohocken, Philadelphia, 2019. https://doi.org/10.1520/C0192_C0192M-19.
[68] ASTM C109/C109M–20b, Standard Test Method for Compressive Strength of Hydraulic Cement Mortars (Using 2-in. or [50 mm] Cube Specimens) 2020 West Conshohocken, Philadelphia 10.1520/C0109_C0109M-20B.
[69] ASTM C642-13, Standard Test Method for Density, Absorption, and Voids in Hardened Concrete, West Conshohocken, Philadelphia, 2013. https://doi.org/10.1520/C0642-13.
[70] BS EN 772-11:2011, Methods of test for masonry units Part 11: Determination of water absorption of aggregate concrete, autoclaved aerated concrete, manufactured stone and natural stone masonry units due to capillary action and the initial rate of water absorption of clay ma, London, UK, 2011. https://doi.org/BS 772.
[71] C. Gorse, D. Johnston, M. Pritchard, A Dictionary of Construction, Surveying and Civil Engineering, Oxford University Press, 2012 doi: 10.1093/acref/9780199534463.001.0001.
[72] ASTM C597–16, Standard Test Method for Pulse Velocity Through Concrete, ASTM International 2016 West Conshohocken, Philadelphia 10.1520/C0597-16.
[73] ASTM C805/C805M-18, Standard Test Method for Rebound Number of Hardened Concrete, ASTM International 2018 West Conshohocken, Philadelphia doi: 10.1520/C0805_C0805M-18.
[74] R. Rostami, M. Zarrebini, K. Sanginabadi, D. Mostofinejad, S. Mahdi Abtahi, H. Fashandi, An investigation into influence of physical and chemical surface modification of macro-polypropylene fibers on properties of cementitious composites, Constr. Build. Mater. 244 (2020) 118340, https://doi.org/10.1016/j.conbuildmat.2020.118340.
[75] R. Ranade, M.D. Stults, B. Lee, V.C. Li, Effects of fiber dispersion and flaw size distribution on the composite properties of PVA-ECC, RILEM Bookseries 2 (2012) 107–114, https://doi.org/10.1007/978-94-007-2436-5_14.
[76] A. Abrishambaf, M. Pimentel, S. Nunes, Influence of fibre orientation on the tensile behaviour of ultra-high performance fibre reinforced cementitious composites, Cem. Concr. Res. 97 (2017) 28–40, https://doi.org/10.1016/j.cemconres.2017.03.007.
[77] B. Çomak, A. Bideci, Ö. Salli Bideci, Effects of hemp fibers on characteristics of cement based mortar, Constr. Build. Mater. 169 (2018) 794–799, https://doi.org/10.1016/j.conbuildmat.2018.03.029.
[78] B. Ren, J. Noda, K. Goda, Effects of fiber orientation angles and fluctuation on the stiffness and strength of sliver-based green composites, J. Soc. Mater. Sci. Jpn. 59 (7) (2010) 567–574, https://doi.org/10.2472/jsms.59.567.
[79] D.D. Chung, Dispersion of short fibers in cement, J. Mater. Civ. Eng. 17 (4) (2005) 379–383, https://doi.org/10.1061/(ASCE)0899-1561(2005)17:4(379).
[80] D.D.L. Chung, Composite Materials: Science and Applications, Springer, London, 2010 doi: 10.1007/978-1-84882-831-5.
[81] S.K. Kirthika, S.K. Singh, Experimental investigations on basalt fibre-reinforced concrete, J. Inst. Eng. (India) Ser. A. 99 (4) (2018) 661–670, https://doi.org/10.1007/s40030-018-0325-4.
[82] Z. Guo, C. Wan, M. Xu, J. Chen, Review of basalt fiber-reinforced concrete in china: alkali resistance of fibers and static mechanical properties of composites, Adv. Mater. Sci. Eng. 2018 (2018) 1–11, https://doi.org/10.1155/2018/9198656.
[83] X. Zhang, X. Zhou, H. Ni, X. Rong, Q. Zhang, X. Xiao, H. Huan, J.F. Liu, Z. Wu, Surface modification of basalt fiber with organic/inorganic composites for biofilm carrier used in wastewater treatment, ACS Sustain. Chem. Eng. 6 (2) (2018) 2596–2602, https://doi.org/10.1021/acssuschemeng.7b04089.
[84] V. Ramakrishnan, N.S. Tolmare, V.B. Brik, Performance evaluation of 3-D Basalt fibre reinforced concrete Basalt rod reinforced concrete, NCHRP-IDEA Program Project Final Report. (1998).
[85] S.T. Kang, B.Y. Lee, J.-K. Kim, Y.Y. Kim, The effect of fibre distribution characteristics on the flexural strength of steel fibre-reinforced ultra high strength concrete, Constr. Build. Mater. 25 (5) (2011) 2450–2457, https://doi.org/10.1016/j.conbuildmat.2010.11.057.
[86] S. Yan, H. Jiao, X. Yang, J. Wang, F. Chen, Bending properties of short-cut basalt fiber shotcrete in deep soft rock roadway, Adv. Civ. Eng. 2020 (2020) 1–9, https://doi.org/10.1155/2020/5749685.
[87] J.V. Jenifer, D. Brindha, J.V. Jenifer, D. Brindha, Development of hybrid steel-basalt fiber reinforced concrete – In aspects of flexure, fracture and microstructure, Rev. La Constr. 20 (2021) 62–90, https://doi.org/10.7764/RDLC.20.1.62.
[88] V.C. Khed, B. Mohammed, M.S. Liew, W. Alaloul, B.S. Mohammed, S. Liew, W. S. Alaloul, M. Adamu, Hybrid fibre rubberized ECC optimization for modulus of elasticity, Int. J. Civil Eng. Technol. 9 (2018) 918–928 (accessed April 23, 2021), http://www.iaeme.com/IJCIET/index.asp918http://www.iaeme.com/ijciet/issues.asp?JType=IJCIET&VType=9&IType=7http://www.iaeme.com/IJCIET/issues.asp?JType=IJCIET&VType=9&IType=7.
[89] B.S. Mohammed, V.C. Khed, M.S. Liew, Optimization of hybrid fibres in engineered cementitious composites, Constr. Build. Mater. 190 (2018) 24–37, https://doi.org/10.1016/j.conbuildmat.2018.08.188.

[90] W. Yin, T.T.C. Hsu, Fatigue behavior of steel fiber reinforced concrete in uniaxial and biaxial compression, ACI Mater. J. 92 (1995) 71–81. https://doi.org/10.14359/1415.
[91] M. Kamal, M. Khan, S.W. Shahzada, K. Alam, Experimental investigation of the mechanical properties of Engineered Cementitious Composites (ECC), Int. J. Adv. Struct. Geotech. Eng. 5 (2016) 40–45.
[92] Ü. Aslan, M., Güler, O., Kaya, M., Alver, The Effect of Basalt Fiber Content on the Physical-Mechanical Properties of the Basalt Fiber Reinforced Polylactic Acid (PLA) Composites., in: II. International Defense Industry Symposium, Kırıkkale, Turkey, 2017: pp. 621–626.
[93] E. Booya, H. Ghaednia, S. Das, H. Pande, Durability of cementitious materials reinforced with various Kraft pulp fibers, Constr. Build. Mater. 191 (2018) 1191–1200, https://doi.org/10.1016/j.conbuildmat.2018.10.139.
[94] E. Güneyisi, M. Gesoğlu, E. Booya, K. Mermerdaş, Strength and permeability properties of self-compacting concrete with cold bonded fly ash lightweight aggregate, Constr. Build. Mater. 74 (2015) 17–24, https://doi.org/10.1016/j.conbuildmat.2014.10.032.
[95] N.S. Martys, C.F. Ferraris, Capillary transport in mortars and concrete, Cem. Concr. Res. 27 (5) (1997) 747–760, https://doi.org/10.1016/S0008-8846(97)00052-5.
[96] W.P.S. Dias, Reduction of concrete sorptivity with age through carbonation, Cem. Concr. Res. 30 (8) (2000) 1255–1261, https://doi.org/10.1016/S0008-8846(00)00311-2.
[97] M. Singh, B. Saini, H.D. Chalak, Long term evaluation of engineered cementitious composite containing stone slurry powder, Constr. Build. Mater. 264 (2020) 120183, https://doi.org/10.1016/j.conbuildmat.2020.120183.
[98] A. Adesina, S. Das, Influence of glass powder on the durability properties of engineered cementitious composites, Constr. Build. Mater. 242 (2020) 118199, https://doi.org/10.1016/j.conbuildmat.2020.118199.
[99] O.R. Alonge, M.B. Ramli, T.J. Lawalson, Properties of hybrid cementitious composite with metakaolin, nanosilica and epoxy, Constr. Build. Mater. 155 (2017) 740–750, https://doi.org/10.1016/j.conbuildmat.2017.08.105.
[100] R. Ralegaonkar, H. Gavali, P. Aswath, S. Abolmaali, Application of chopped basalt fibers in reinforced mortar: a review, Constr. Build. Mater. 164 (2018) 589–602, https://doi.org/10.1016/j.conbuildmat.2017.12.245.
[101] W.J. Leslie, J.R. Cheesman, An ultrasonic method of studying deterioration and cracking in concrete structures, J. Am. Concr. Inst. 21 (1949) 17–36.
[102] J. Elena, M. Daniela Lucia, X-ray diffraction study of hydration processes in the Portland cement, J. Appl. Eng. Sci. 1 (2011) 79–86.
[103] S.A. Abo-El-Enein, A.H. Ali, F.N. Talkhan, H.A. Abdel-Gawwad, Application of microbial biocementation to improve the physico-mechanical properties of cement mortar, HBRC J. 9 (1) (2013) 36–40, https://doi.org/10.1016/j.hbrcj.2012.10.004.
[104] E. Booya, K. Gorospe, H. Ghaednia, S. Das, Durability properties of engineered pulp fibre reinforced concretes made with and without supplementary cementitious materials, Compos. B Eng. 172 (2019) 376–386, https://doi.org/10.1016/j.compositesb.2019.05.070.
[105] H. Liu, G. Luo, H. Wei, H. Yu, Strength, Permeability, and Freeze-Thaw Durability of Pervious Concrete with Different Aggregate Sizes, Porosities, and Water-Binder Ratios, Applied Sciences 2018, Vol. 8, Page 1217. 8 (2018) 1217. https://doi.org/10.3390/APP8081217.